Study of the Deactivation of Methanol Synthesis Catalysts

EPRI

EPRI AF-694
Project 779-12
Final Report
May 1978

Keywords:
Coal Liquefaction
Synthetic Fuels
Methanol
Reaction Kinetics
Catalyst Development

Prepared by
Lehigh University
Bethlehem, Pennsylvania

ELECTRIC POWER RESEARCH INSTITUTE

Study of the Deactivation of Methanol Synthesis Catalysts

AF-694
Research Project 779-12

Final Report, May 1978

Prepared by

Center for Surface and Coatings Research
LEHIGH UNIVERSITY
Sinclair Laboratory, Building #7
Bethlehem, Pennsylvania 18015

Principal Investigators
Kamil Klier
Richard G. Herman

Prepared for

Electric Power Research Institute
3412 Hillview Avenue
Palo Alto, California 94304

EPRI Project Managers
Howard E. Lebowitz
Ronald H. Wolk
Fossil Fuel and Advanced Systems Division

ABSTRACT

This report summarizes the progress made under the seven month project "Study of the Deactivation of Methanol Synthesis Catalysts," which was supported by the Electric Power Research Institute by Contract Number RP 779-12. A brief review on the commercial production of methanol is presented, as well as a commentary on the use of methyl fuel by the electric utility companies.

During this project, sets of reference, used, and deliberately poisoned Cu/Zn/Al catalysts were examined by Auger and X-ray photoelectron (XPS) spectroscopies, and the surface areas and pore size distributions were determined. These catalysts were obtained from Chem Systems Inc., who are developing a methanol conversion process based on a liquid phase reactor for EPRI under contract number RP 317-2. Methods for sample preparation for the surface analyses of catalysts taken from the liquid phase process were developed. Massive contamination occurred with both sulfur and chlorine on samples exposed to 5 ppm H_2S or 10 ppm CH_3Cl; their surface areas decreased significantly but the pore size distributions were not altered. In comparison, the surface areas of the deactivated catalysts (Nos. 11 and 13) were a maximum of only 10-15% lower than the surface areas of the reference catalysts and of the used active catalysts. XPS and Auger analyses did not detect any major differences between the active catalysts and the deactivated catalysts; all contained traces of sulfur, chlorine, and perhaps nickel. Since the sensitivity of XPS-Auger analyses is 1% of surface concentration, these results indicate that the catalysts (11 and 13) were deactivated by minute quantities of undetected impurities other than sulfur and chlorine, or by an impurity removed with the white oil during sample preparation, or by a reaction that transfers copper from the proposed active Cu^+/ZnO phase (cf. below) into the inactive metal Cu(0) phase. A deactivation mechanism such as the

latter was indicated by a separate experiment in which a laboratory prepared $Cu/ZnO/Al_2O_3$ catalyst suffered an irreversible loss of activity upon over-reduction. The final proof for over-reduction could be obtained by combined UPS and optical measurements.

Preparation and characterization of a series of binary CuO/ZnO catalysts yielded additional insights into the mechanism of methanol synthesis and of catalyst deactivation. Following either simple reduction or catalytic testing, the catalysts, particularly the lower copper-containing preparation, exhibited a black absorption edge in the neighborhood of 15,000 cm^{-1}. The intensity of this absorbance paralleled the catalytic activity of the lower copper-containing catalysts. The absorption edge is assigned to Cu^+ in solid solution with ZnO. It is proposed that this moiety activates CO and determines the catalytic activity of methanol synthesis catalysts. The single phase catalysts that were prepared contain only a small concentration of this active species but display a significant low pressure activity. Poisoning of the active sites by sulfur- and chlorine-containing compounds can occur through complexation of a number of catalyst components, but the copper species are considered most susceptible to attack by H_2S and Cl compounds. There are indications that COS in low concentrations behaves as a promoter of the synthesis rather than as a poison.

TABLE OF CONTENTS

Blank Page

LIST OF FIGURES

LIST OF TABLES

I. SUMMARY

The primary objective of the research was to investigate the causes of deactivation of Cu/Zn/Al and Cu/Zn/Cr methanol synthesis catalysts encountered in industrial and laboratory practice. Emphasis was placed on the physical examination of both the unused and the used catalysts, such that carbon deposits, chemical contamination, changes in chemical composition, and loss of active surface area would be readily noted. To aid in the interpretation of results, simplified binary catalysts composed of CuO/ZnO were prepared and studied. The research program was divided into four tasks and summaries of the results from each of the tasks are presented below.

Task 1. Eight catalyst samples were received from Chem Systems, Inc. Four were used catalysts from methanol conversion tests, two were deliberately poisoned samples and two were unused reference samples. Six catalysts were coated with white mineral oil since that was the medium used during the liquid phase methanol synthesis testing. A procedure involving extraction and vacuum drying was developed for removing the oil from the catalyst pellets. All of the catalysts were examined by XPS and Auger Spectroscopy and the surface areas and pore size distributions were determined. The surface areas of the poisoned catalysts were lower than those of the reference and used samples. XPS indicated that all of the copper was in the zero-valent or monovalent state, and the Auger data showed that the surface layers of the used catalysts were in general zinc-rich, which was in contrast to the bulk data obtained after crushing the catalyst pellets.

Task 2. A series of 12 catalysts was prepared in which the weight % CuO in the CuO/ZnO samples was varied from 0 to 100. It was found that the catalyst precursors, as precipitated, could form 3-phase systems; the pure copper sample (100:0) precipitated as $Cu_2(OH)_3NO_3$

and the pure zinc sample (0:100) precipitated as $Zn_5(OH)_6(CO_3)_2$, while the mixed samples (e.g. 50:50) contained various amounts of $(Cu,Zn)_2(OH)_2CO_3$ as a third component. Following calcination to the oxides, scanning transmission electron microscopy (STEM) demonstrated that there were two ranges of ZnO morphologies; a needle-like morphology existed between 0 and 30% CuO, while hexagonal platelets were observed between 40 and 100% CuO.

A maximum in the activity for methanol synthesis was observed at the catalyst composition of CuO/ZnO = 30:70. This corresponded to the maximum surface area and to the maximum intensity of an optical absorption edge at about 15,000 cm^{-1} observed for this system of catalysts. X-ray fluorescence, in conjunction with STEM, indicated that the zinc oxide crystallites in the tested catalysts contained over 10% copper (% of metal content). Considering the XPS data, it is proposed that the copper is present in the zinc oxide in the univalent oxidation state as a solid solution.

A synthesis mechanism for the conversion of CO and H_2 into methanol (CH_3OH) is proposed whereby the Cu^+ centers in the zinc oxide nondissociatively chemisorb and activate carbon monoxide, while the ZnO surface dissociatively activates the hydrogen. The observed rate enhancing effect of CO_2, H_2O, and O_2 is due to the maintenance of an oxidation potential high enough to keep the copper in the active centers as Cu^+.

Task 3. Attempts to prepare single phase catalysts, e.g. solid solutions of copper in zinc oxide, were made. Samples corresponding to 2:98, 5:95, and 10:90 CuO/ZnO were coprecipitated. Upon calcination to 900°C, the 2% CuO sample formed a Cu^{2+}/ZnO solid solution, but the 5% preparation appeared to yield CuO, as well as the solid solution. Manual mixing of the pure components in proportions to yield 5:95 did not produce a single phase solid solution after calcination at 900°C for 48 hours. The 2:98 catalyst exhibited a definite, but low, catalytic activity for methanol synthesis when it was calcined only to 350°C prior to reduction and testing at 250°C.

Task 4. A preliminary poisoning study was carried out at 100 atm and 250°C utilizing a Cu/Zn/Cr catalyst. In the usual synthesis gas stream of $H_2/CO/CO_2$ = 70:24:6 vol %, gradual but steady deactivation occurred. Addition of 2 ppm COS to the synthesis gas did not further deactivate the catalyst, but rather, it stabilized the catalytic conversion. In fact, an increase in the catalytic activity was noted.

II. INTRODUCTION

BACKGROUND OF METHANOL SYNTHESIS

The impetus behind the current research program at Lehigh University on methanol synthesis catalysis is our conclusion that, among energy resources, methanol is probably the most versatile in scope. It can be synthesized from a large range of materials, e.g. wood, biomass, natural gas, coal, petroleum products, and atmospheric carbon dioxide. Besides its use as a primary solvent and as a feedstock for the manufacture of plastics and aliphatics, methanol is used or is projected for use as follows:

1. Automotive fuel,
2. Fuel for peak electric power generation,
3. Replacement of coke in the manufacture of steel,
4. Source of pure hydrogen, e.g., in fuel cells,
5. Feedstock for single cell protein (SCP) production,
6. Alkylation and solubilization of coal,
7. Substitute for propane in LPG applications,
8. Ethylene production via ethanol synthesis,
9. Transportation medium for coal in slurry pipelines, and
10. Direct conversion into gasoline.

Upon consumption as a pure energy chemical, methanol is non-polluting and exhibits low corrosiveness.

At the present time, methanol is catalytically produced from synthesis gas (equation 1), most of which is obtained by partial oxidation or steam reforming

$$CO + 2H_2 \rightarrow CH_3OH \qquad (1)$$

of natural gas. Although natural gas is a rather pure source of synthesis gas, the quantity available for new or expanded uses is

and will continue to be very limited. To illustrate this point, it can be noted that the U.S. production of natural gas leveled off during the period 1971-1973 at 637 $\pm$ 3 billion m^3 of gas [1]. By 1976, the production had dropped to about 538 billion m^3/year [2]. The Federal Energy Administration has forecast that natural gas production will decrease to approximately 480 billion m^3/year by 1985 if price regulation is continued, but if there is deregulation, as well as completion of the Alaskan gas pipeline, natural gas production could approach that obtained during the 1971-1973 period [2]. If industry accelerates its exploration and developmental off-shore program, the U.S. outer continental shelf might supply a maximum addition of about 70 billion m^3 of natural gas per year in 1985 [3].

The conclusion is that the synthesis gas required for the increasing production of methanol will be obtained by the gasification of coal. A major difficulty in conjunction with this arises from the fact that coal is a complex mixture of polymers that is heavily contaminated with metals, as well as with non-metals such as sulfur and the halogens. Upon gasification, the non-metals are volatilized and are carried along with the synthesis gas stream. The volatile impurities must usually be removed because they are corrosive and, as the following discussion will show, often behave as catalyst poisons.

The formation of methanol according to equation 1 is thermodynamically favored by low temperatures and high pressures. Prior to the mid-1960's, methanol synthesis catalysts consisted of mixtures of zinc oxide and chromia (Cr_2O_3). To obtain reasonable conversions to methanol, e.g. 5-10%, temperatures in the range of 350-400°C were needed, which necessitated the use of pressures in the range of 300-350 atm. It was subsequently found that copper-based catalysts promoted with zinc oxide and chromia or alumina were much more active, and this allowed lower temperatures, e.g. 250°C, and lower pressures (50-100 atm) to be used. While the ZnO-Cr_2O_3 catalyst is rather insensitive to sulfur-poisoning, the copper-based catalyst is extremely sensitive to the presence of sulfur compounds in the synthesis gas. For the latter catalyst, the synthesis gas has to be purified to a level below 0.1 ppm

sulfur by a multi-step adsorption procedure or by a Sulfinol or Rectisol purification process.

The purification step following gasification is very important from an economic viewpoint since the raw gas from a Kopper-Totzek gasifier utilizing U.S. coals typically contains 0.3-2% H_2S and 0.02-0.2% COS [4]. There are definite economic advantages to the low pressure methanol synthesis, e.g. lower compression and pipework costs, that mitigate against the use of the high pressure methanol synthesis catalyst.

FUEL GRADE METHANOL FOR ELECTRIC POWER GENERATION

Fuel-grade methanol contains appreciable quantities of higher alcohols in addition to methanol. This fuel would probably be used for power generation, rather than pure methanol, because it has a higher caloric content and would be more economical than methanol. It could be used for firing steam boilers in electric utility, industrial, and institutional power generation, or it could be used directly to drive gas turbines.

In the first category, a large scale demonstration using methanol to generate electricity was carried out in September 1972 at the New Orleans Public Service A. B. Paterson Station using a commercial 50 megawatt capacity utility boiler [5-7]. The test was sponsored by Southern California Edison Company, Consolidated Edison Company (New York), New Orleans Public Service, Inc., and Vulcan-Cincinnati, Inc. In comparison to natural gas and to fuel oil, methanol burned more efficiently and yielded less nitrogen oxides and carbon monoxide. In addition, no sulfur compounds or particulates were emitted [7].

The usage of gas turbines for electric power generation has steadily increased in recent years. This growth parallels the increase in the number of hours of peak shaving required by the major utility companies, since the turbines are generally used as auxiliary power units. During the hours of peak demand, methanol could be fed to the auxiliary gas turbines for the production of the required

electricity. The feasibility of using methanol directly as a fuel for peak shaving gas turbines has been successfully demonstrated [8]. The fuel, of course, could be delivered to the power station by pipeline, rail, or barge. Alternatively, if coal is the fuel used to generate electricity, a portion of the synthesis gas produced during the gasification could be diverted, desulfurized, and converted into methanol [9]. Thus, a constant stream of coal could be fed to the electric power station; during low demand periods, e.g. the middle of the night, methanol would be synthesized and stored, while during periods of peak load requiring peak shaving the methanol would be used to generate electric power via the gas turbines. Major utility companies that supply their base loads from large capacity nuclear power stations could still take advantage of methanol driven gas turbines. During off-peak periods, methanol could still be generated from coal and stored, while coal, rather than fuel oil, would be used for intermediate loads [8].

Advantages of fuel grade methanol over current fuels for gas turbines include the following:

1. lower output of nitrogen oxides due to the lower flame temperature,
2. lower or no output of sulfur-containing pollutants,
3. lower compression horsepower requirements, and
4. lower blade erosion and deposit rates due to the absence of metallic elements.

In regard to the fourth point, it has been estimated that due to the cut-back in "corrosion", less maintenance would be required and the time between overhauls of the turbines could be tripled [7, 10].

To complete this discussion, it must be recognized that the problem of catalyst poisoning by sulfur during the synthesis of methanol from the generated synthesis gas is still to be faced. The stream of synthesis gas still has to be purified to below 0.1 ppm sulfur before undergoing catalytic conversion to methanol over the present-day low pressure copper-based catalyst. This is much less than the maximum allowable exposure for employees (8-hour weighted average) of 20 ppm set by the Occupational Safety and Health Administration [11, 12]. It is also much lower than the current

on-site environmental standard (Clean Air Act) for coal-based power generation stations. The maximum allowable sulfur content is 1.2 lb SO_2 in the stack gas per million Btu of coal consumed. This converts to approximately 0.2 vol % H_2S in the synthesis gas. Thus, it is evident that the sulfur limits are set by the catalyst sensitivity and not by environmental and safety standards.

RESEARCH OBJECTIVES AND PLAN

The primary objective of this research was to investigate the cause of deactivation of Cu/Zn/Al and Cu/Zn/Cr methanol synthesis catalysts encountered in industrial and laboratory practice. Emphasis was placed on the physical examination of both the unused and the used catalysts, so that carbon deposits, chemical contamination, changes in chemical composition, and loss of active surface area could be readily noted. To aid in the interpretation of results, the simplified binary system composed of CuO/ZnO was prepared and studied.

The research plan was divided into the following tasks:

1. Commercial catalysts tested by Chem Systems, Inc. in a liquid phase methanol synthesis process were characterized. Two of the Cu/Zn/Al catalysts had undergone successful testing [13], two were tested catalysts that had become deactivated, two were poisoned samples, and two were unused reference samples. The surface and bulk compositions were analyzed by Auger and X-ray Photoelectron (XPS) Spectroscopies. Surface areas and pore size distributions were determined by the Argon adsorption isotherms and related calculations.

2. A series of Cu/ZnO catalysts were prepared by coprecipitation from nitrate solution by using Na_2CO_3 as the precipitating agent. Changes in the catalytic activity were determined as a function of the CuO/ZnO ratio in the calcined, but unreduced, catalysts. The tested catalysts were characterized by X-ray powder diffraction, optical spectroscopy, and X-ray fluorescence combined with scanning and transmission electron microscopy, as well as by the tools listed under Task 1.

3. Studies of model systems involving single phase catalysts were initiated at a lower level of effort. These catalysts were based on solid solutions of various metal oxides and sulfides in ZnO and ZnS.

4. Poisoning experiments using H_2S and/or COS at 100 ppm (and lower) levels were performed with a Cu/Zn/Cr catalysts that had been previously characterized. After partial deactivation of the catalyst had been achieved, the effect of 2 ppm COS was determined. Characterization of the used catalysts will be carried out.

III. DISCUSSION OF RESULTS

A. TASK 1: CATALYSTS FROM CHEM SYSTEMS, INC.

Experimental

The eight catalysts received from Chem Systems, Inc. were commercial Cu/Zn/Al catalysts that were purchased by Chem Systems. All of them contained approximately 2% carbon, which acted as a lubricant when the catalysts were pelletized from dry powders. A description of the catalysts is given in Table 1.

In the particular Chem Systems reactor used for deactivation studies, the catalyst bed is centered in the reactor by means of layers of glass beads above and below the bed, which is flooded by white oil. The gas flow is downward through the reactor, in contrast to the earlier experiments by Chem Systems [13]. The reaction temperature was precisely maintained by means of a molten salt bath that surrounded the reactor. A typical charge of catalyst was 33.2 g, which was the charge used with catalysts 20-C and 21-C. During the poisoning studies, the nominal gas composition was 33% N_2, 34% H_2, 17% CO, 7% CO_2, and 9% CH_4, where the gas space velocity was approximately 100 l/hr. In the chlorine poisoning experiment, 10 ppm CH_3Cl was added to the feed gas. To accomplish the sulfur poisoning, 5 ppm H_2S by volume was maintained in the synthesis gas. The duration of the poisoning runs were 1000-1500 hr. It should be noted that the catalysts were in operation for 4000-5000 hr prior to the addition of the trace poisons to the systems.

Extraction of the white oil. Upon receiving the used catalysts at Lehigh University, a procedure was established for removing the white oil from the samples by extraction in a Soxhlet extractor. Using about 2 g of oil-soaked material (placed in a 1.5 x 7 cm Soxhlet thimble), the 125 ml of cyclohexane used as the solvent was refluxed such that the extraction thimble was filled every 20

TABLE 1

Cu/Zn/Al CATALYSTS FROM CHEM SYSTEMS, INC.

CATALYST NUMBER	PARTICLE SIZE (mm)[a]	REDUCTION TIME (DAYS)	TREATMENT
5	2.4 x 2	0	Unused
7	6.4 x 3	0	Unused
9	16-20 Mesh	1	Used
10	2.4 x 2	1	Used
11	2.4 x 2	4	Used[b]
13	2.4 x 2	1	Used[b]
20-C	6.4 x 3	?	Chlorine poisoned
21-C	6.4 x 3	?	Sulfur poisoned

a) Tablets (diameter x height), except for Catalyst Number 9

b) Deactivated after prolonged use.

minutes. After the extraction was carried out for 5 hours, the catalyst was placed in a small bottle of clean cyclohexane and allowed to stand overnight. Following decantation of the solvent, the solid was washed three times with 10 ml portions of petroleum ether (20°-40°C boiling fraction). Extraction with the latter solvent was then carried out for 2 hours, at which time the solvent was replaced with fresh petroleum ether. Following 4 hours of additional extraction, the catalyst was removed from the thimble and was rinsed with three 10 ml portions of petroleum ether. The sample was then vacuum dried to remove any adhering solvent.

After this extraction process, no residual oil could be detected by infrared spectroscopy, as is shown in Figure 1. Spectrum A was obtained after wiping the excess oil off the catalyst pellets, pulverizing the tablets, and then mulling with hexachlorobutadiene (HCB). To determine the sensitivity of the infrared analysis, a small quantity of white oil was accurately weighed, mixed with three drops of HCB, and mulled with a weighted amount of oil-free

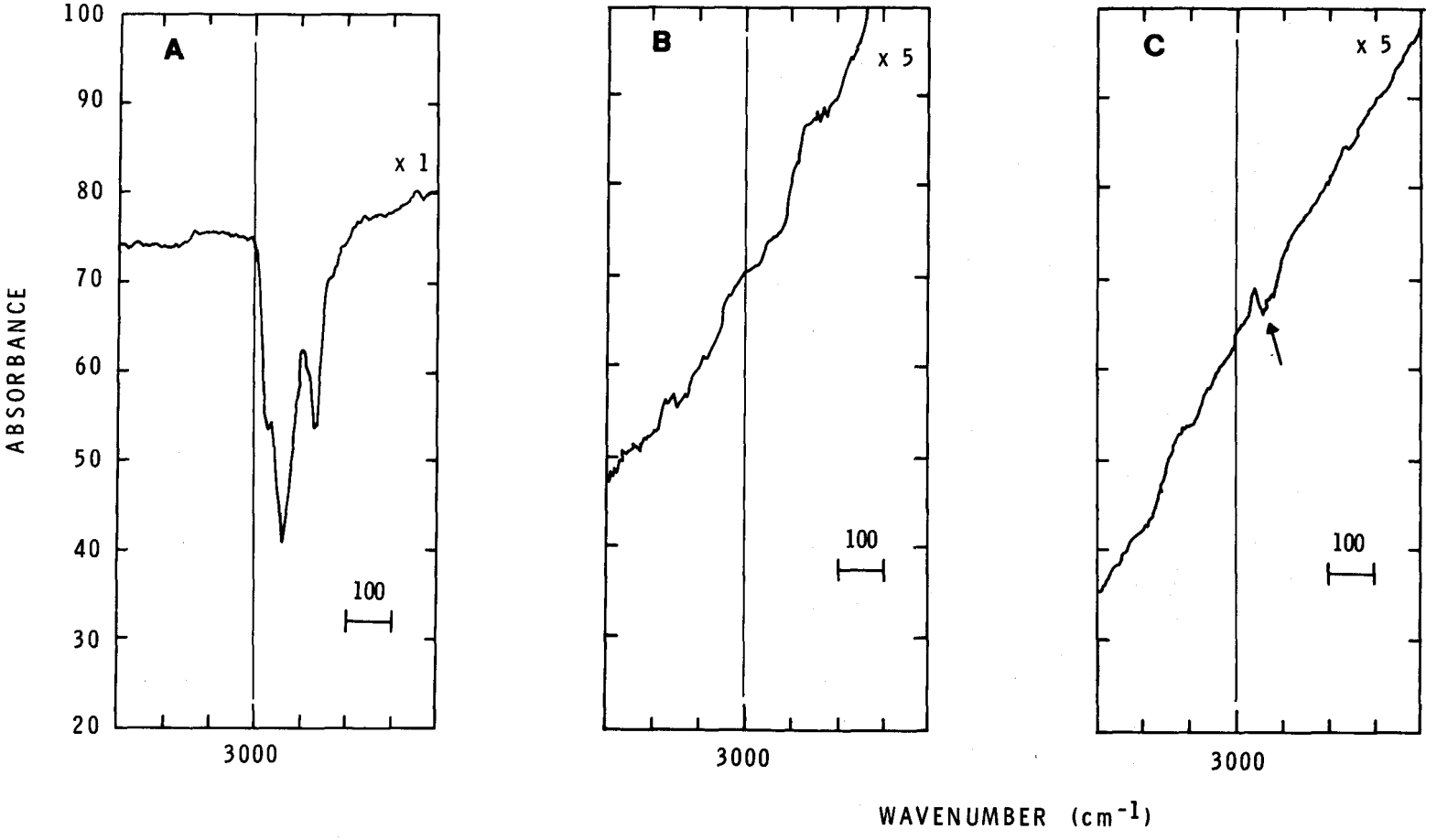

Figure 1. The infrared spectra of Chem Systems Cu/Zn/Al catalysts: (A) Oil-saturated Catalyst No. 13, (B) Extracted Catalyst No. 13, and (C) Reference Catalyst No. 7 containing 0.7 wt % white oil. These were obtained as mulls with hexachlorobutadiene.

reference catalyst No. 7. It is evident in Figure 1C that 0.7 wt % of white oil on the catalyst is clearly detectable.

Auger and X-ray photoelectron spectroscopic analyses. The Auger analyses were carried out in the Physical Electronics Auger Spectrometer (Phi Model 50-220) equipped with a cylindrical mirror analyzer. The catalyst samples were exposed to air, pressed into an indium foil and inserted into the sample holder. Following evacuation, the analyses were carried out with particular attention to Cu, Zn, O, Cr, Al, Ni, Fe, C, S, Cl, Na, and Ca. The X-ray photoelectron analyses were performed using the Physical Electronics ESCA-Auger Spectrometer Model 548. The sample preparation was the same as for the Auger analyses.

Surface areas and pore distribution determinations. A standard BET method was used for the determination of surface areas from argon adsorption at -195°C. An argon area of 16.8 $Å^2$ was used in the calculations of monolayer areas.

The mesopore distribution was determined by analysis of the adsorption-desorption isotherms based on Brunauer's corrected modelless method and its analytical modification [14]. The micropore volume was calculated according to Sing [15], where the shape of the experimental isotherm is compared with that of a standard isotherm obtained on a reference non-porous material (chromia gel).

Hydrogen reductions. Prior to being characterized, the reference catalysts Nos. 5 and 7 were reduced in a stream of 2% H_2 - 98% N_2. The catalysts were first dehydrated at 200°C under flowing N_2. After changing the gas stream to the reducing mixture (GHSV = 1375 hr^{-1}), the catalysts were reduced at 250°C for 14 hours. After being cooled, the samples were transferred to small bottles and were stored briefly under nitrogen before undergoing analysis.

Results

The argon adsorption-desorption isotherms were obtained for all eight Cu/Zn/Al catalysts, and all of the isotherms were of the same general shape and exhibited the same amount of hysteresis. The

isotherms for the reference catalysts and for the poisoned catalysts are shown in Figure 2. It is evident from the figure that the surface areas of the poisoned catalysts are appreciably lower than are those of the reference catalysts. The calculated surface areas, including those of the used catalysts, are compiled in Table 2.

TABLE 2

THE SURFACE AREAS OF THE Cu/Zn/Al CATALYSTS [CHEM SYSTEMS, INC.]

CATALYST NUMBER	SURFACE AREA (m^2/g)
5	99.8
10	95.6
11	83.7
13	85.7
7	88.0
9	90.6
20-C	45
21-C	67

An analysis of the mesopore volume distribution, assuming cylindrical pores, was carried out for each catalyst. The distribution curves for the four catalysts referred to in Figure 2 are shown in Figure 3, where the mesopores are the intermediate size pores having radii in the 1.5-20 nm range. For comparison, the distribution curve obtained for a Cu/Zn/Al = 60:30:10 catalyst prepared at Lehigh University is shown. Following a 10-fold magnification, the shape of the latter curve is found to be the same as for the commercial catalysts. The mesopore volume distribution curves for the two active used catalysts and for the two deactivated catalysts are exhibited in Figure 4. It can be noted that catalysts 9 and 10 contain a significant number of pores having diameters in the 8 to 24 nm range.

Auger analysis of the reduced reference catalysts showed nothing un-

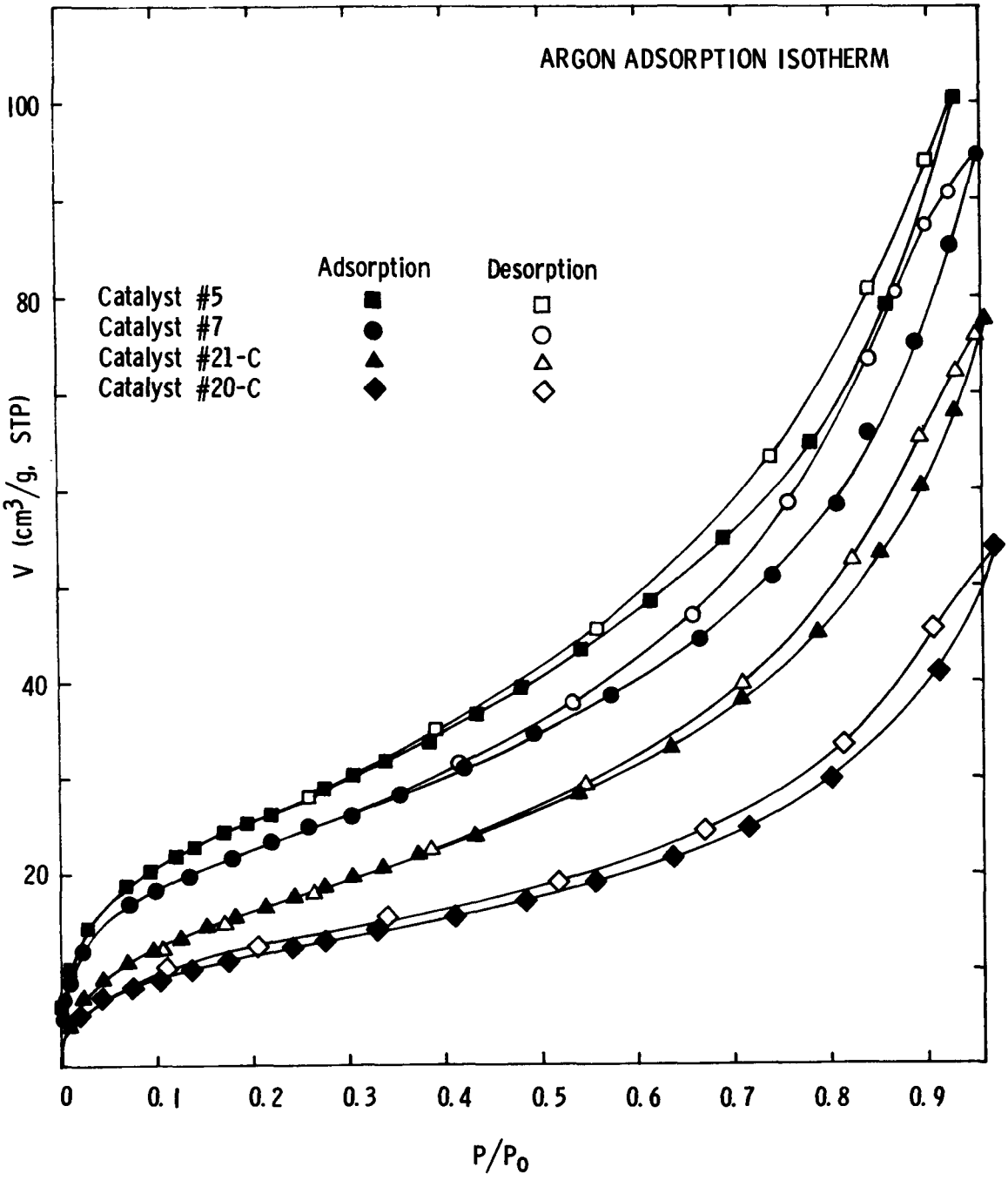

Figure 2. The Argon adsorption-desorption isotherms determined for the reference catalysts (Nos. 5 and 7) for the poisoned catalysts (Nos. 20-C and 31-C).

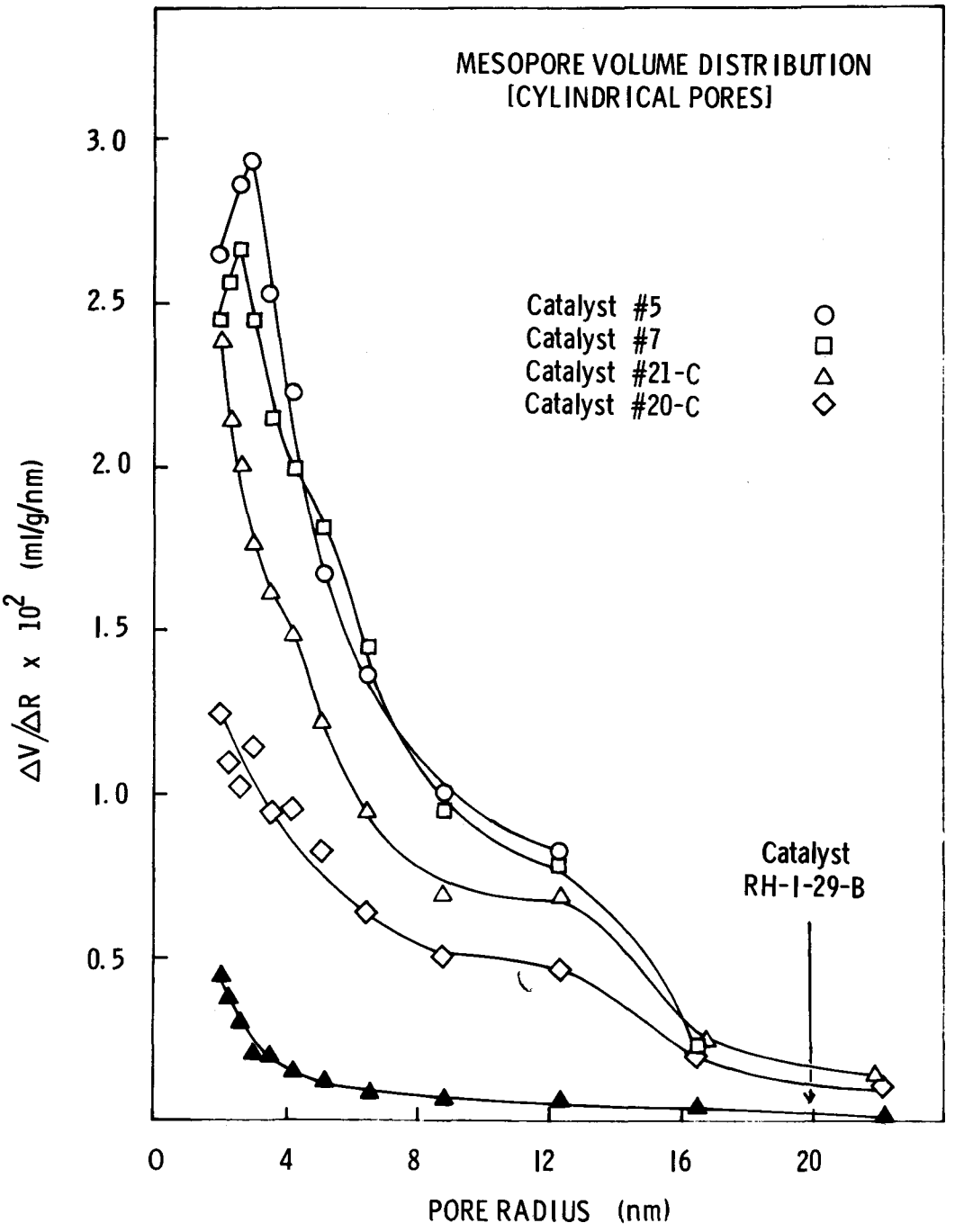

Figure 3. The mesopore volume distribution curves for the reference catalysts (Nos. 5 and 7) and for the poisoned catalysts (Nos. 20-C and 21-C).

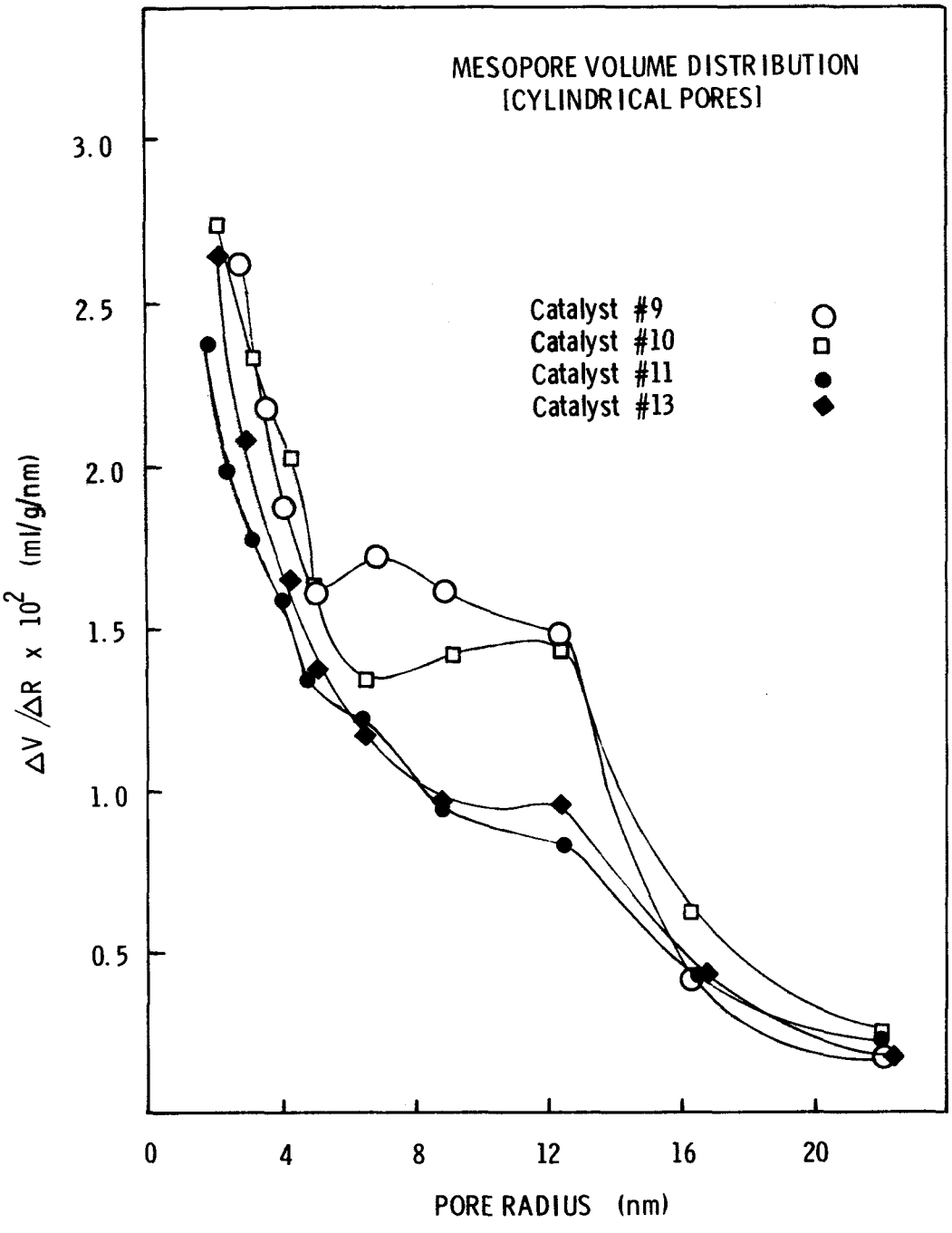

Figure 4. The mesopore volume distribution curves for the Chem Systems used Cu/Zn/Al catalysts.

expected. The spectra were clear and showed the absence of Na, Ca, S, and Cl. Analysis by XPS demonstrated, by line position, that copper was present in the materials as Cu^{+} and/or Cu^{0}, but not as Cu^{2+}. The Auger spectra of the poisoned catalysts confirmed the presence of the poisons in appreciable quantities. The spectrum of catalyst 20-C is shown in Figure 5. It is evident that this catalyst is very heavily chlorinated, and that the chlorine (chloride) is not withdrawn from the solid in the high vacuum of the Auger spectrometer. No evidence for the presence of iron is visible (iron would exhibit three lines of equal intensity between the oxygen and copper sets of lines). However, the surface of the glass beads associated with the used catalyst was covered with large amounts of both iron and chlorine. It can be noted from Figure 5 that carbon has evidently been removed from the catalyst.

In Figure 6 is the Auger spectrum of the sulfur-poisoned catalyst. A strong line due to sulfur is visible, as well as a line corresponding to chlorine. This poisoning experiment was carried out in a different reactor than was the chlorine poisoning test. Again, there is no evidence of the presence of iron in the catalyst, and XPS indicated that copper was present as Cu^{+}. The indium lines, are, of course, due to the supporting foil.

The active (Nos. 9 and 10) and deactivated (Nos. 11 and 13) catalysts were studied in a more systematic way by Auger Spectroscopy. At least two samples of each catalyst were examined; one consisted of a carefully powdered sample while the other was a whole pellet mounted in the vacuum chamber. The powdered samples yielded bulk analyses, that is the analyses of the internal volume of the catalysts. The Auger spectra of the whole pellets yielded information in regard to the surface composition. Figure 7 shows the spectrum for a powdered sample of catalyst No. 11, and this is representative for catalysts 10 and 13 also. Traces of S and Cl are visible, although none were added to the synthesis gas. The major copper line is more intense than are the zinc and aluminum lines, as expected. It is possible, although not definite due to peak overlap, that a trace of nickel is also present in the catalyst. For comparison, the Auger spectra obtained from the face of pellets

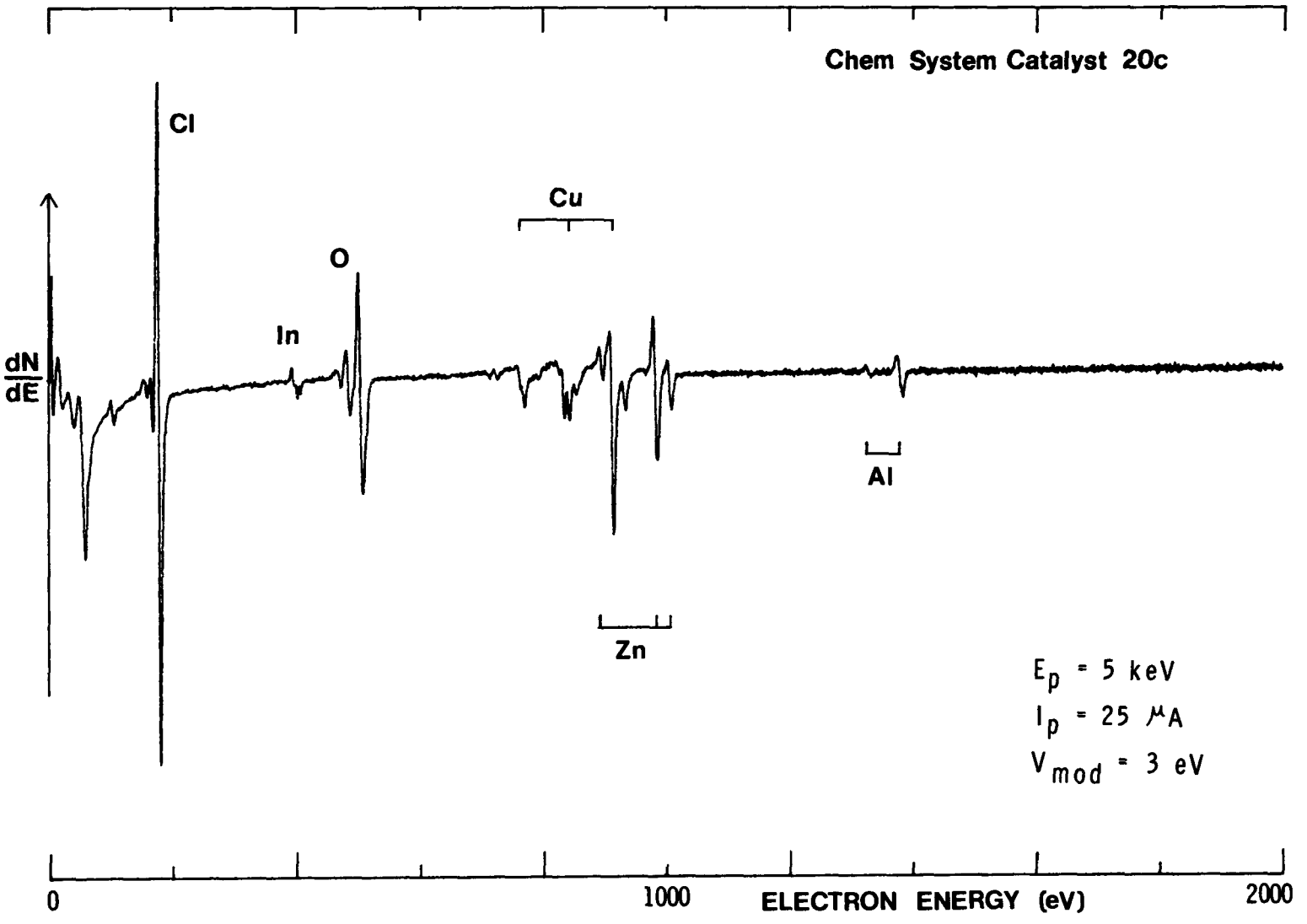

Figure 5. The Auger spectrum of catalyst No. 20-C that had been poisoned by 10 ppm CH_3Cl.

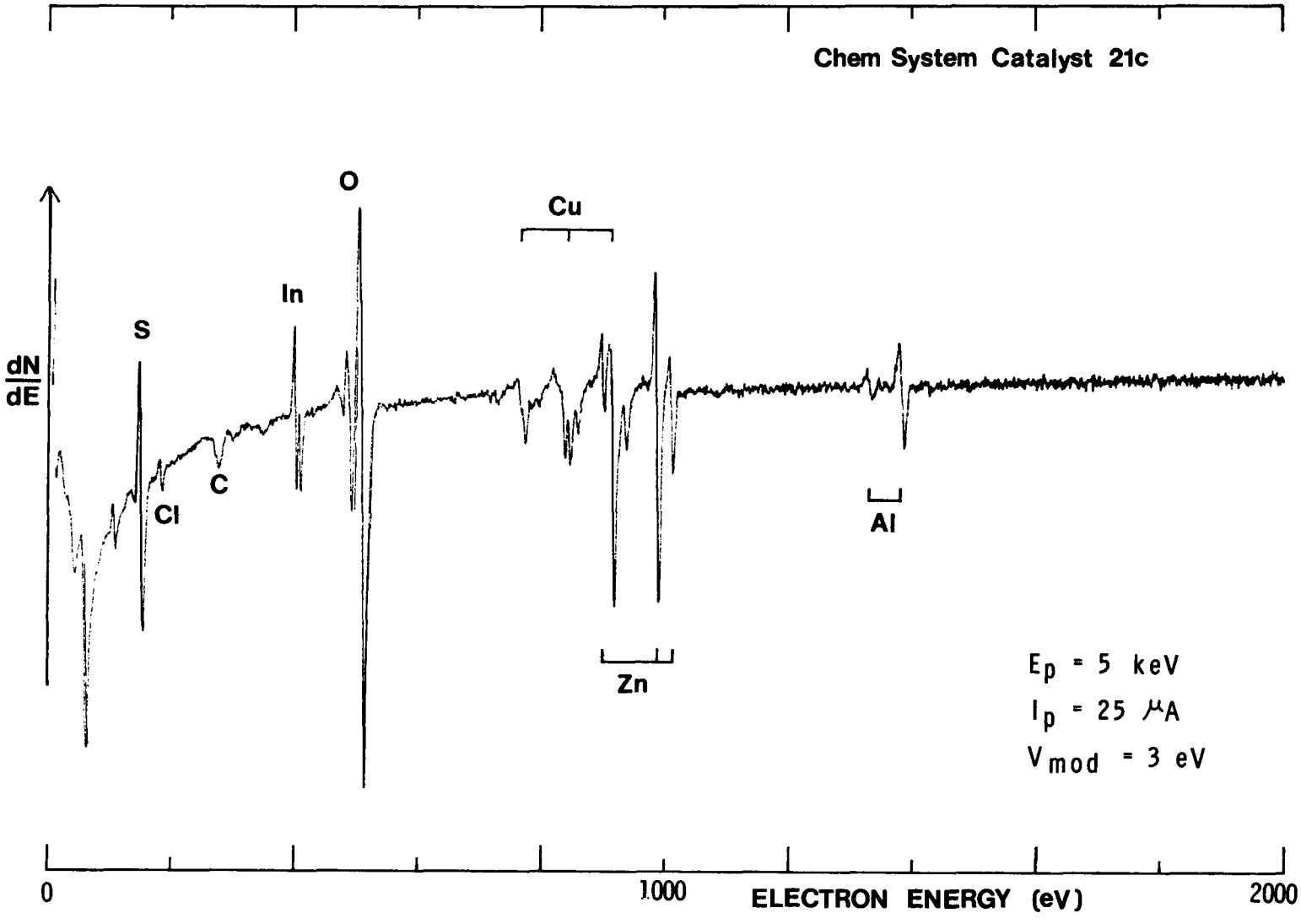

Figure 6. The Auger spectrum of catalyst No. 21-C that had been poisoned by 5ppm H_2S.

of catalysts 11, 10, and 13 are shown in Figures 8-10.

Discussion

It was found that the extraction procedure developed at Lehigh University to remove the white oil from the catalyst pellets used in the liquid phase methanol synthesis testing was successful. The infrared band due to the white oil disappeared after extraction (see Figure 1B). During surface area measurements, no interference by white oil was observed. In addition, the Auger spectra were reproducible in regard to the carbon line, and XPS indicated the presence of only one type of carbon (graphitic carbon). In the case of a carbon-clean catalyst, no residue carbon due to the white oil was noted (Figure 5).

The volumetric gas adsorption-desorption experiments demonstrate that the Chem Systems Cu/Zn/Al catalysts exhibit similar behavior and contain mesopores of similar size. As noted in Table 2 and for Figure 2, the surface areas of the poisoned catalysts were only 50-70% of those of the non-poisoned samples. The poisoning decreased the number of pores but not the distribution of the existing pores, as is shown in Figure 3. It is interesting that Catalysts No. 9 and 10 exhibit an enhanced number (volume) of mesopores of intermediate size (Figure 4). While the Catalyst No. 9 sample consisted of 16-20 Mesh particles and the other samples were pelletized, Catalysts 9, 10 and 13 were reduced for one day and then tested in the synthesis gas system previously described. Thus, the cause for the increase in the number of intermediate mesopores in Catalysts 9 and 10 is not evident.

The chlorine-poisoned catalyst exhibited the lowest surface area of those submitted by Chem Systems. Besides showing that the catalyst is very heavily chlorinated, the Auger spectrum in Figure 5 indicates a low aluminum content (compare with Figures 6-10). In our experience at Lehigh University, much of the surface area of Cu/Zn/Al catalysts is associated with the alumina component. Therefore, in this chlorine-poisoned catalyst, part of the decrease in surface area might be related to the possible loss of the Al_2O_3 component from the catalyst. It is particularly interesting to note that the sublimation temperature of $AlCl_3$ (or Al_2Cl_6) is 177.8°C at

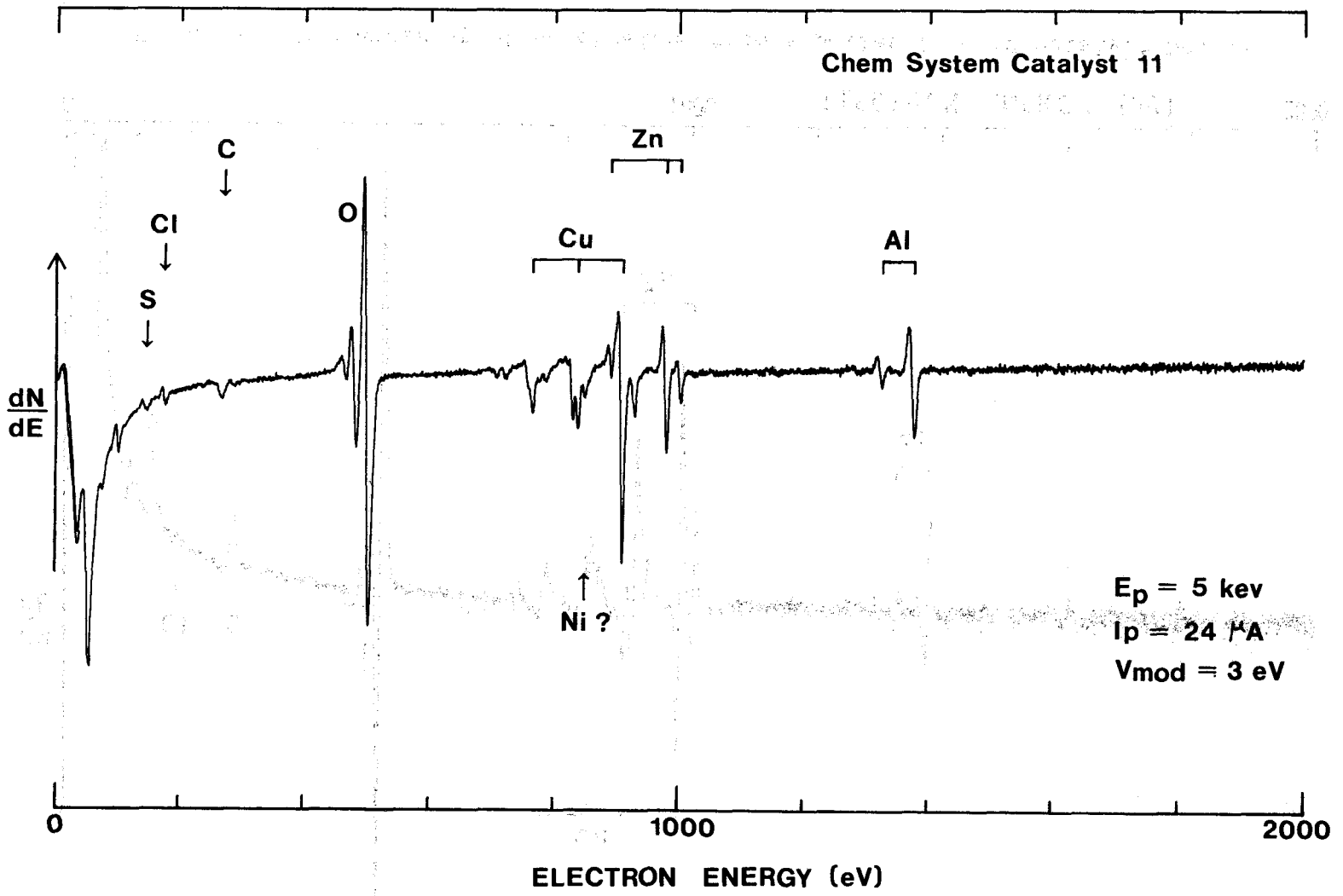

Figure 7. The Auger spectrum of a powdered sample of catalyst No. 11.

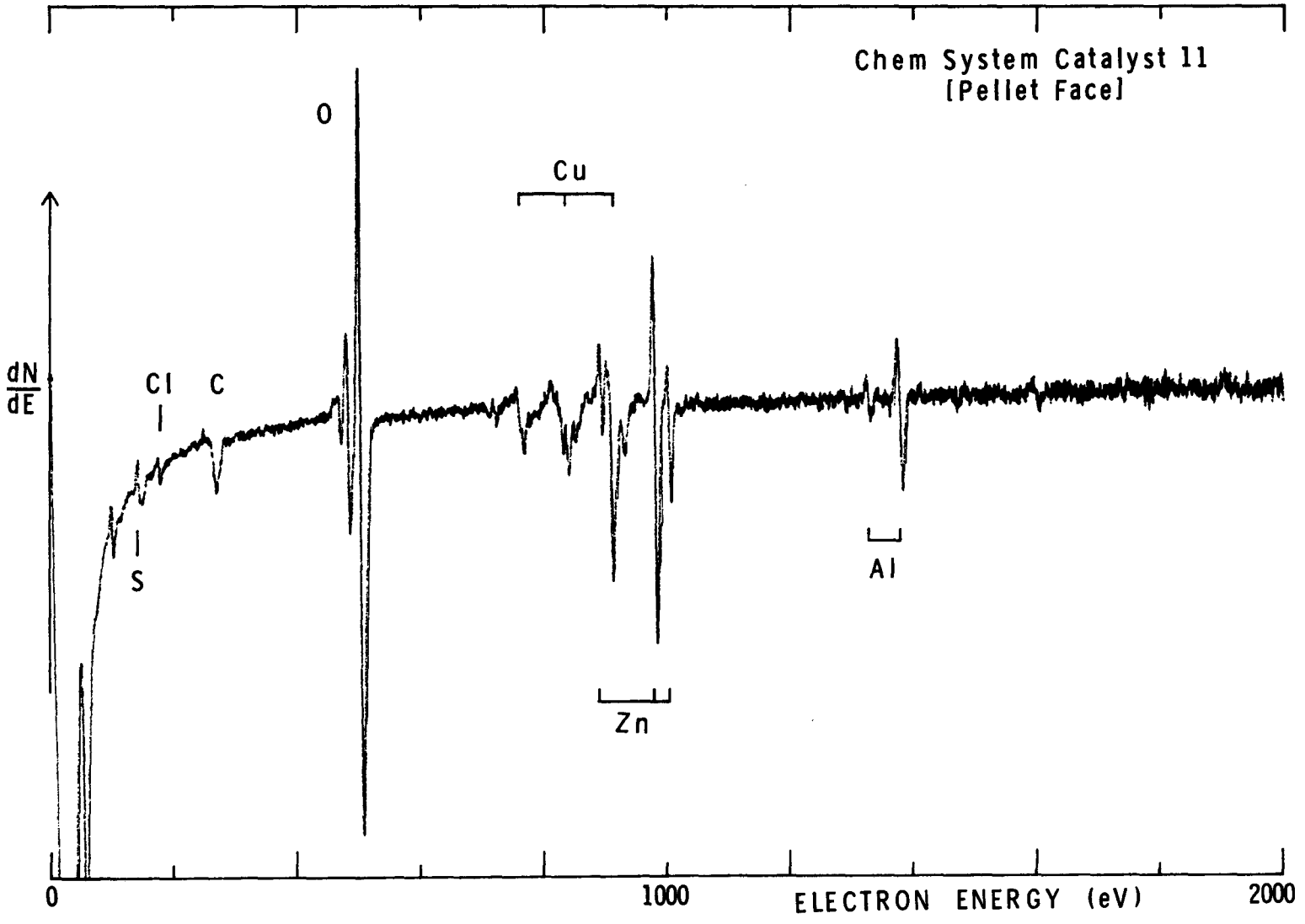

Figure 8. The Auger spectrum obtained from a pellet face of catalyst No. 11.

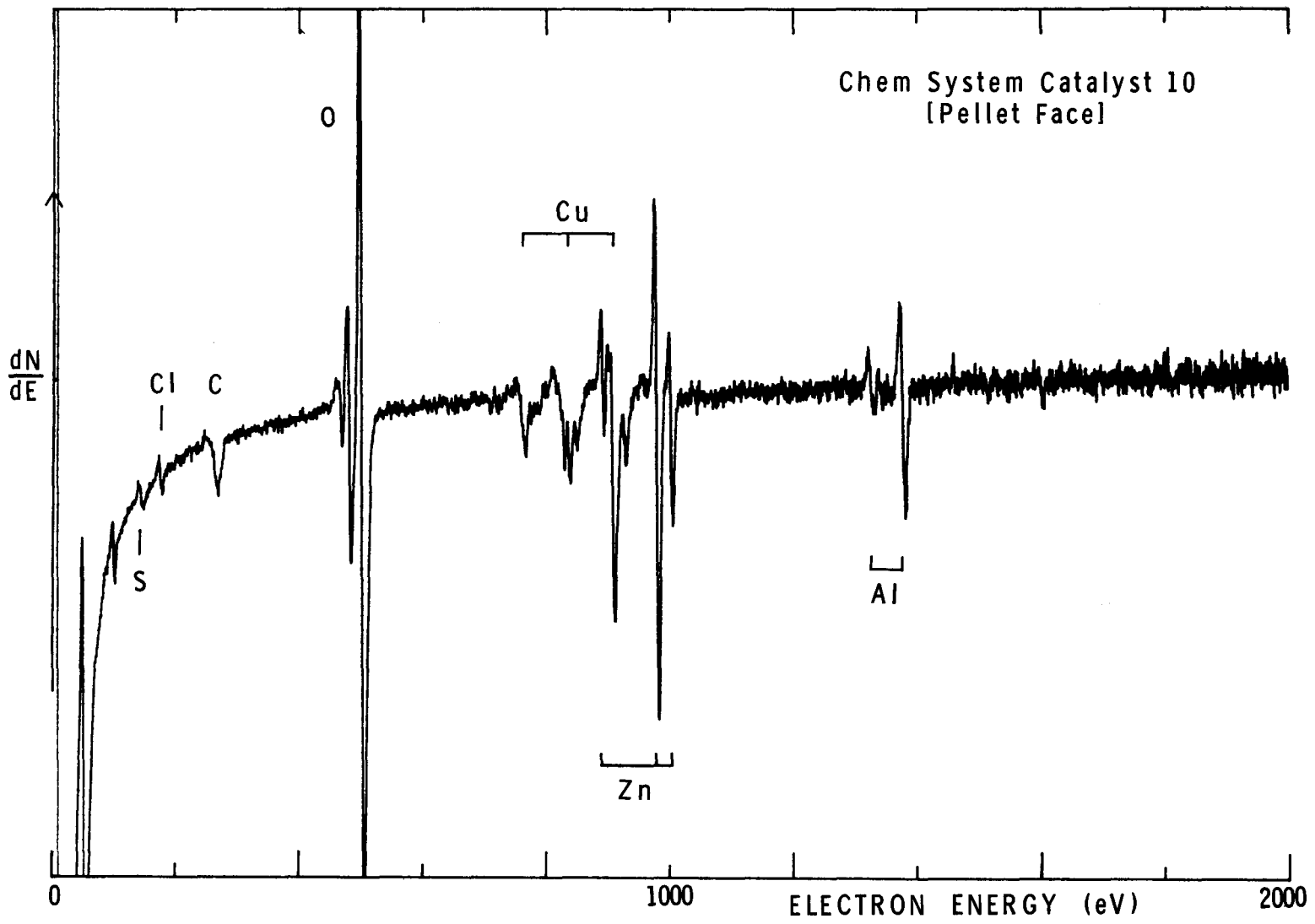

Figure 9. The Auger spectrum obtained from a pellet face of catalyst No. 10.

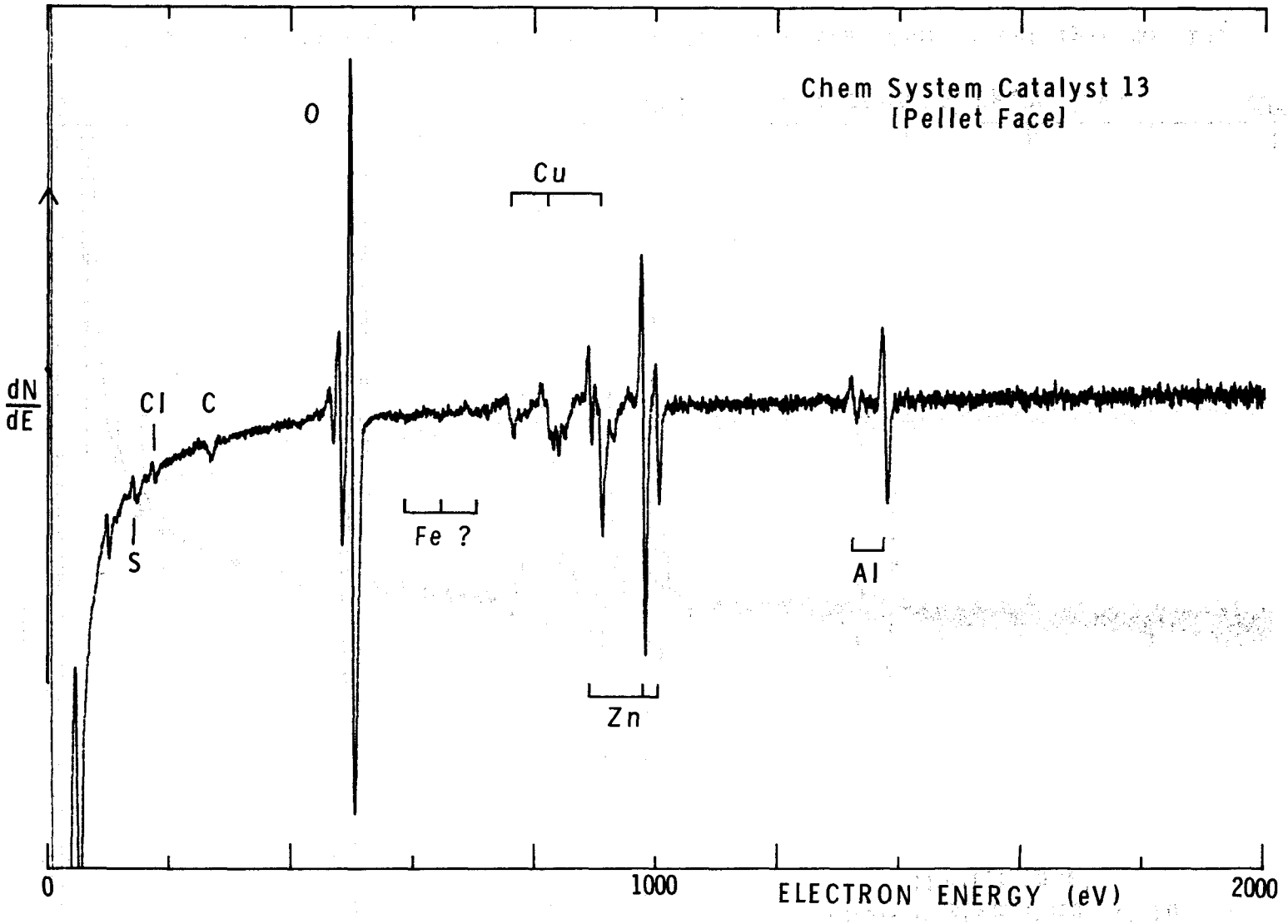

Figure 10. The Auger spectrum obtained from a pellet face of catalyst No. 13.

atmospheric pressure [16].

Due to the large quantity of chlorine present in the catalyst, it would appear that it must also react with the copper and zinc components. In consideration of the data to be presented in the next section of this report under Task 2, it is proposed that the loss of catalytic activity is associated with the reaction of chlorine with Cu and not with the Al moiety. The same is true in the case of sulfur-poisoning, where no formation of volatile components should occur, but the clogging of pores could occur by the formation of sulfides. The mechanism of sulfur-poisoning will be briefly discussed under Task 2.

All of the used catalysts showed traces of sulfur and chlorine, although these were not intentionally added to the reactor system (e.g. see Figures 7-10). It appeared that the surface of Catalyst 13 (Figure 10) contained a trace of iron. For the carefully powdered samples of used catalysts, the intensities of the Cu, Zn, and Al Auger lines bore a direct relationship to the composition of the catalysts. An example is shown in Figure 7. Analysis of the faces of the catalyst pellets yielded a variation in the expected line intensities, however. While the aluminum appeared to be randomly and uniformly distributed throughout the bulk and surface of the catalyst, the surface faces were rich in zinc and deficient in copper (Figures 8-10). This result was very unexpected. However, it is expected that copper will at least partially agglomerate into metallic crystallites upon reduction. During the generation of the Auger spectra, the electron beam might simply have missed the copper-rich (metallic copper particles) areas. An indication of the composition of the zinc-rich surface is provided by the Cu/Zn ratio derived from the intensities of the most intense Auger lines. The ratios calculated from Figures 8-10 fall in the range of 0.38 to 0.56. These can be compared to the ratio of 2.0 derived from Figure 7, which is the expected ratio since most aluminum-based commercial catalysts have initial compositions of $CuO/ZnO/Al_2O_3$ = 60:30:10 wt %. No major differences were noted between the active catalysts and the deactivated catalysts.

Conclusions

The Cu/Zn/Al catalysts received from Chem Systems, Inc. were characterized by surface area measurements, mesopore volume distribution curves, XPS, and Auger Spectroscopy. Effects due to poisoning of the catalysts were noted, but the specific mechanisms of sulfur- and chlorine-poisoning were not established. However, it appeared that sulfide formation, chloride formation, and loss of alumina are contributory factors that decreased the surface area. The Auger spectra showed a difference in the surface composition as compared to the bulk composition of the catalyst pellets. In the future, the external surfaces of the catalyst particles should be analyzed as well as the internal bulk composition.

B. TASK 2: BINARY Cu/ZnO CATALYSTS

The mechanisms, kinetics, and reactive species involved in methanol synthesis and in sulfur- and chlorine-poisoning have not yet been established. An interesting feature of the tertiary catalysts is the fact that the mixed catalyst is at least three orders of magnitude more active than each of the separate catalyst components [17]. To gain insight into the methanol synthesis process, the following pertinent questions were addressed in Task 2:

1. What is the nature and origin of the promotional effect in the mixed catalyst -- are there solid-state compounds formed or is there a special structural feature that makes the mixed catalyst more active and selective than the simple catalyst components?
2. What is the role of oxidizing gases on the reaction mechanism and catalyst performance?
3. What are the reactive species and probable mechanisms involved in methanol synthesis and catalyst deactivation?

To simplify this investigation, binary catalysts rather than tertiary catalysts were prepared, and a detailed characterization using X-ray powder diffraction, optical methods, Auger and X-ray photoelectron spectroscopies, BET-pore distribution measurements, and electron microscopic and microdiffraction techniques was carried out with both tested and unused catalysts.

Experimental

Testing apparatus. The catalyst activity was evaluated in a pressure unit (Figure 11) equipped with a flow reactor and with pressure, flow rate, and temperature controls. The catalytic reactor consisted of 1.27 cm ID, 316 stainless steel tubing fitted with 0.32 cm OD thermowell and a volume permitting the testing of catalyst samples ranging in size from 1.0 cm^3 to 35 cm^3.

Downstream from the reactor, the pressure was reduced to atmospheric by a pressure pilot controlled Research valve, and the product

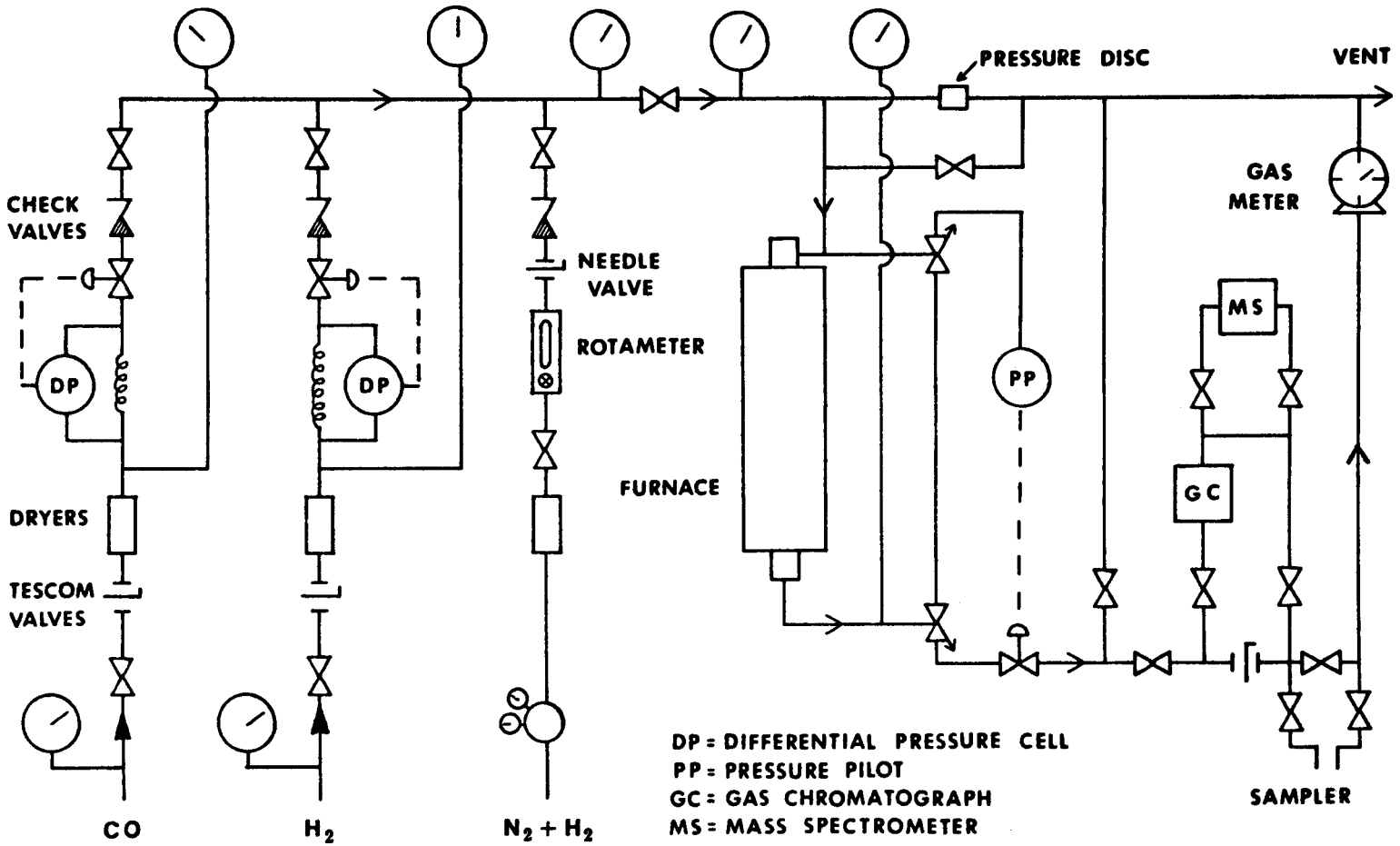

Figure 11. A diagram of the low pressure reaction system used to test methanol synthesis catalysts.

mixture was led through a heated stainless steel tube to the gas sampling valve of a gas chromatograph. The HP 5730A model coupled with a HP 3380A reporting integrator was used for quantitative analysis of the products. All gases used in this work were high purity (CO, CO_2 and O_2 > 99.3%, H_2 > 99.995%) and were obtained, either pure or premixed to desired compositions, from Air Products and Chemicals.

Catalyst preparation. Catalysts were prepared so as to vary the chemical composition from pure components to ternary mixtures in order to identify the compound active in the low pressure methanol synthesis. A series of copper-zinc oxide catalysts with final composition ranging from pure zinc oxide to pure copper was prepared by coprecipitation of basic salts of copper and zinc from approximately 1M nitrate solutions by dropwise addition of 1M sodium carbonate at 85-90°C until the pH was raised from approximately 3 to between 6.8 and 7.0. The reaction typically took 1.5 hr and consumed between 350 and 450 ml of the Na_2CO_3 solution per 1500 ml of the (Cu, Zn) nitrate solution. Following a 1 hr digestion while the solution cooled, the precipitate was collected on a fritted glass filter and was washed thoroughly with distilled water. The samples were then dried overnight at 60-110°C. The subsequent calcination was carried out in air by heating the catalyst sample in a furnace from 150° to 350°C in increments of 50°C every 30 min. X-ray analysis showed a mixture of CuO [18] and ZnO [19] phases. The oxides were pelletized from aqueous slurries, dried at ambient temperature, and then broken to a uniform 10-20 mesh size. The catalyst samples (typically 3 ml) were then placed in the reactor (Figure 11) and reduced in 2% H_2 in N_2 (1 atm) at 245-255°C at a flow rate of approximately 4 l/hr for 4-20 hr. Samples for X-ray diffraction, surface area measurements, Auger spectroscopic and optical measurements were taken before and after the catalyst use and maintained in an N_2 atmosphere to avoid re-oxidation.

X-ray powder diffraction. The powder patterns were obtained by using a Siemens X-ray diffractometer with CuK_α radiation. Samples were slowly exposed to air, mounted on a glass slide using double-

seal tape and inserted into the sample holder. Values for d-spacings listed in reference 20 were used to identify the compounds contributing to the diffraction pattern. After a compound has been identified, its diffraction pattern was computed from the published structure, using the atomic scattering factors [21] and making corrections for multiplicity of reflections, geometrical and polarization factors according to equation (2)

$$I = NK \frac{1}{v^2} |F|^2 p \left[\frac{1 + \cos^2 2\theta}{\sin^2 \theta \cos \theta} \right] \qquad (2)$$

where I is the intensity of an X-ray diffraction line, N is the number of unit cells in the irradiated volume, K is a constant common to all structures, V is the volume of the unit cell, $|F|^2$ is the complex square of the structure factor, p is the multiplicity of the reflection, and the last term is the Lorentz polarization factor [22]. The structure factors of the reflections of each of the investigated compounds were calculated from the tabulated atomic scattering factors. No corrections were made or deemed necessary for absorption of CuK_α radiation in the samples. A comparison of experimental intensities with the calculated ones for all pure compounds investigated here showed an agreement satisfactory for using the X-ray intensities for a quantitative analysis of mixtures. This analysis naturally excludes any amorphous compounds but does account for line broadening due to microcrystallinity by taking areas under the diffraction peaks rather than peak heights as a measure of diffraction intensities.

XPS, Auger analysis, surface areas, and pore distribution determinations. These analyses were carried out using the procedures that were described under Task 1.

Optical spectroscopy. Optical measurements were carried out by diffuse reflectance in Cary 17I or Cary 14R spectrometers in the range of wavelengths from 240 nm to 2400 nm, covering UV, visible, and near-infrared regions. The samples were placed in silica front window cells [23] without exposure to air, either by transfer under nitrogen or by a direct reduction in a closed system con-

taining the optical cell by a procedure identical to that described in the Catalyst Preparation section above.

Results

Phase Composition of the Catalyst Precursors and of the Catalysts.

1. The Cu-Zn precipitates. The powder patterns of the precipitates from Cu-Zn nitrate solutions showed the presence of three compounds, $Cu_2(OH)_3NO_3$(I), $Zn_5(OH)_6(CO_3)_2$(II), and $(Cu, Zn)_2(OH)_2CO_3$(III). The relative proportions of these compounds were determined by the initial Cu:Zn ratio in the solution. The diffraction patterns of compounds I, II, and III accounted for all the lines in each of the mixed precipitates. Figure 12 shows the relative abundances N_i of compounds I, II, and III, calculated from the observed diffraction intensities I_i according to equation (2) in which the structure factor was determined from the published structures of compounds I [24], II [25], and III [26] and the atomic scattering factors as outlines in the Experimental section.

2. Calcined CuO-ZnO samples. After the final calcination step at 350°C (3 hrs.), all mixed precipitates of compounds I, II, and III formed a two-phase system consisting of hexagonal ZnO [19] and tetragonal CuO [18] of relative abundances as shown in Figure 13. Beginning with 15% CuO/85% ZnO, the samples showed 2-4% less than the theoretical amount of CuO. This result suggests that 2-4% of CuO is dissolved in ZnO. Further evidence of solution of Cu in ZnO has been obtained from electron induced X-ray fluorescence analysis in the scanning transmission electron microscope [27]. Although the concentrations of the crystalline phases of CuO and ZnO vary uniformly throughout the whole compositional range, there are two ranges of ZnO morphologies, one between 0 and 30% CuO, in which the ZnO crystallites appear in the form of needles or rods with their sixfold crystal axis parallel to the major dimensions, and another between 40 and 67% CuO, in which the ZnO crystallites are hexagonal platelets with the sixfold crystal axis perpendicular to the major dimensions [27].

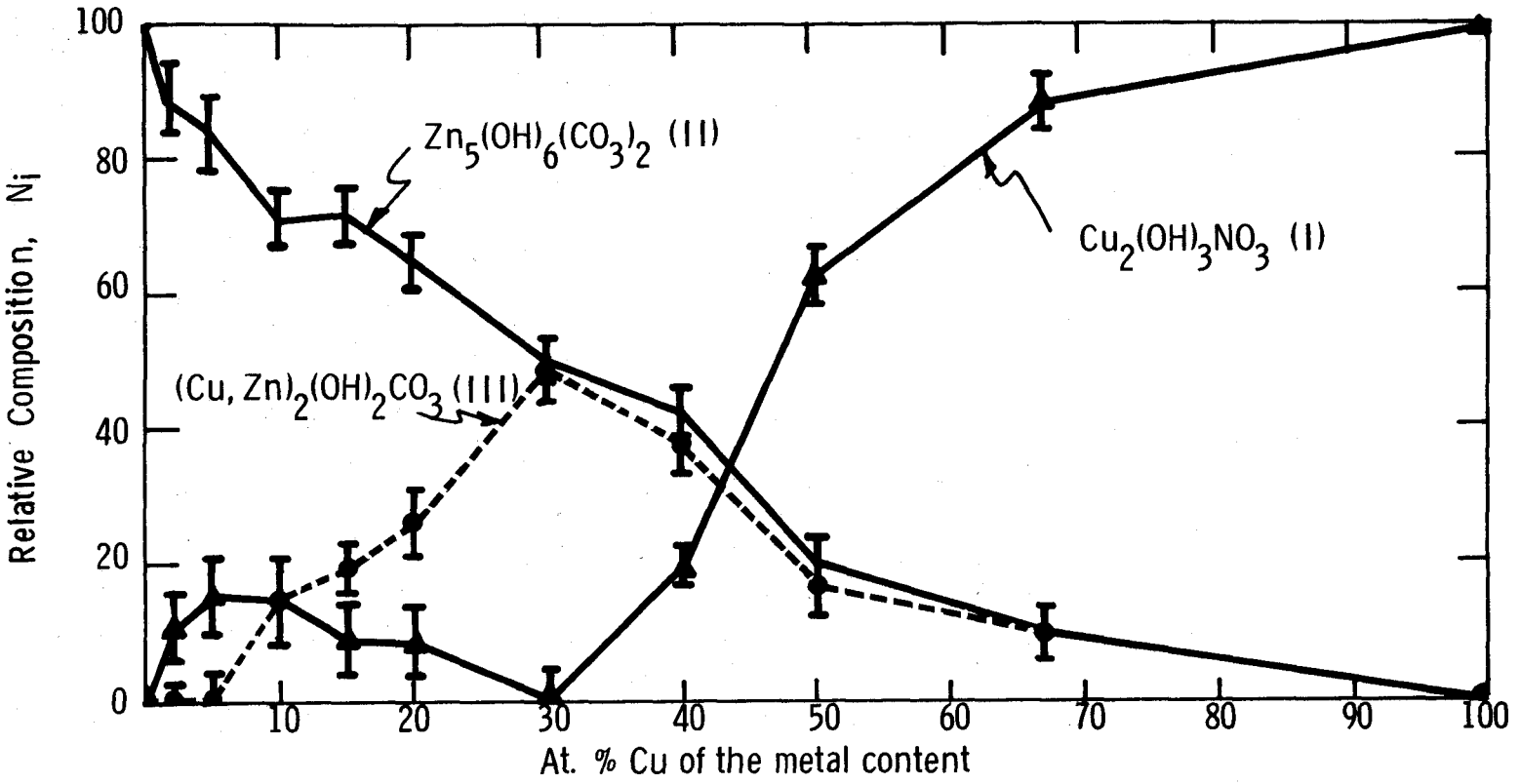

Figure 12. The compositional profile of the Cu-Zn system determined by x-ray powder diffraction of the catalyst precursors formed from nitrate solution by carbonate precipitation.

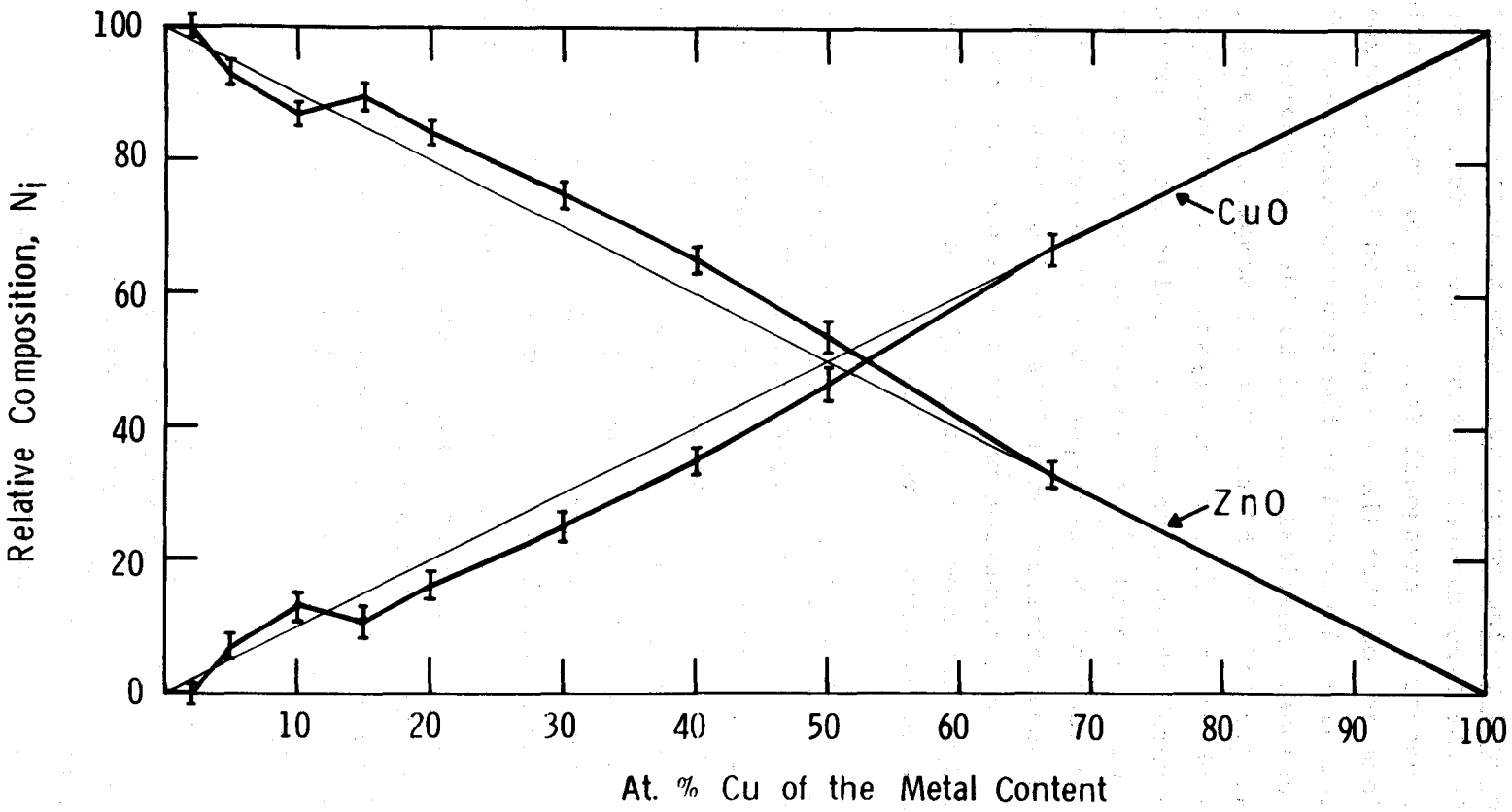

Figure 13. The compositional profile determined by x-ray powder diffraction following calcination of the Cu-Zn precursor samples to 350°C.

3. Reduced and used Cu-ZnO catalysts. Upon reduction at conditions specified in the Experimental section, the product consisted of metallic copper and hexagonal ZnO. Electron microscopic investigations showed that the ZnO particles did not change their crystal habit described in the previous paragraph while the copper assumed spherical (for 10 to 40% CuO samples) or irregular blunted (for 50 to 100% CuO samples) shapes [27]. Neither the phase composition nor crystallite morphology of the reduced catalysts changed upon a regular use in methanol synthesis under the conditions reported in this work. The phase compositions of the catalyst precursors and the calcined, reduced, and used catalysts were determined by X-ray powder diffraction. The diffraction patterns obtained with the Cu/Zn = 67:33 catalyst are shown in Figure 14. The patterns for the reduced and used catalysts were identical.

Surface Composition of the Catalyst Precursors and of the Catalysts. Surface analysis of selected catalyst precursors, reduced catalysts, and used catalysts was carried out by X-ray photoelectron and Auger spectroscopies. The precipitate precursors containing 5, 30, and 67% Cu were subject to XPS/Auger analysis which showed all the expected elemental constituents and no impurities such as S, Cl, Na, and Ca. More detailed analysis of the 67% Cu sample provided evidence of two superimposed oxygen 1s peaks, a major one at 535 eV and a minor one at 529 eV. A significant carbon 1s but only a very small nitrogen 1s peak were observed despite the large quantity of nitrate in the sample, indicating that the nitrate groups were not on the surface; in view of this observation the 535 eV oxygen peak is assigned to hydroxyl and the small shoulder at 529 eV to carbonate oxygen [28].

Particular attention was paid to tracing carbon during the catalyst preparation and use. Figure 15 shows the Auger spectra of a calcined (A) and used (B) $Cu/ZnO/Cr_2O_3$ catalyst demonstrating that the carbon 1s peak, be it residual carbonate or an impurity, disappeared and also that carbon deposits were not formed during the use. The displayed surface analysis was typical of all catalyst preparations studied in the present work including catalysts deactivated by re-

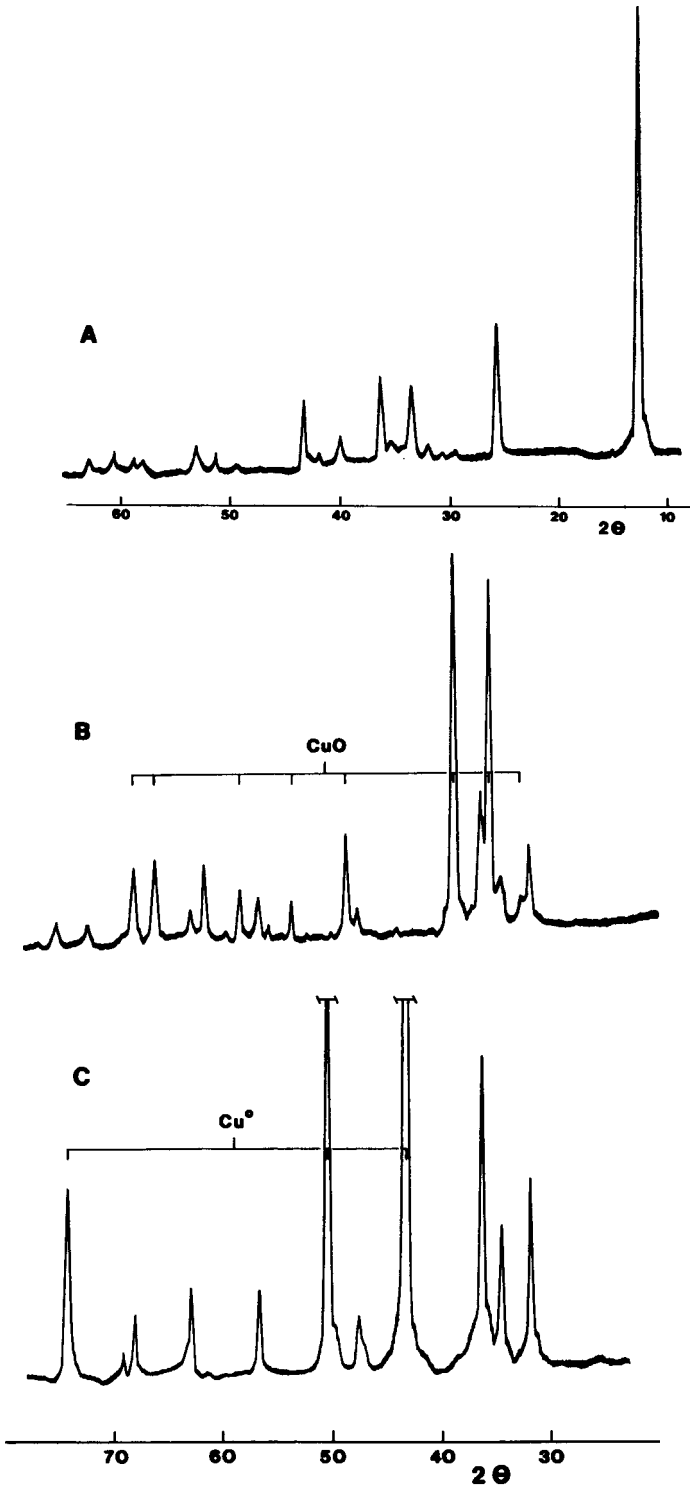

Figure 14. The x-ray powder diffraction patterns of the Cu/Zn (67:33) catalyst (A) after precipitation and drying, (B) after calcination at 350°C, and (C) after being tested for methanol synthesis. The unassigned lines in patterns B and C are due to ZnO. Spectrum A corresponds to $Cu_2(OH)_3NO_3$.

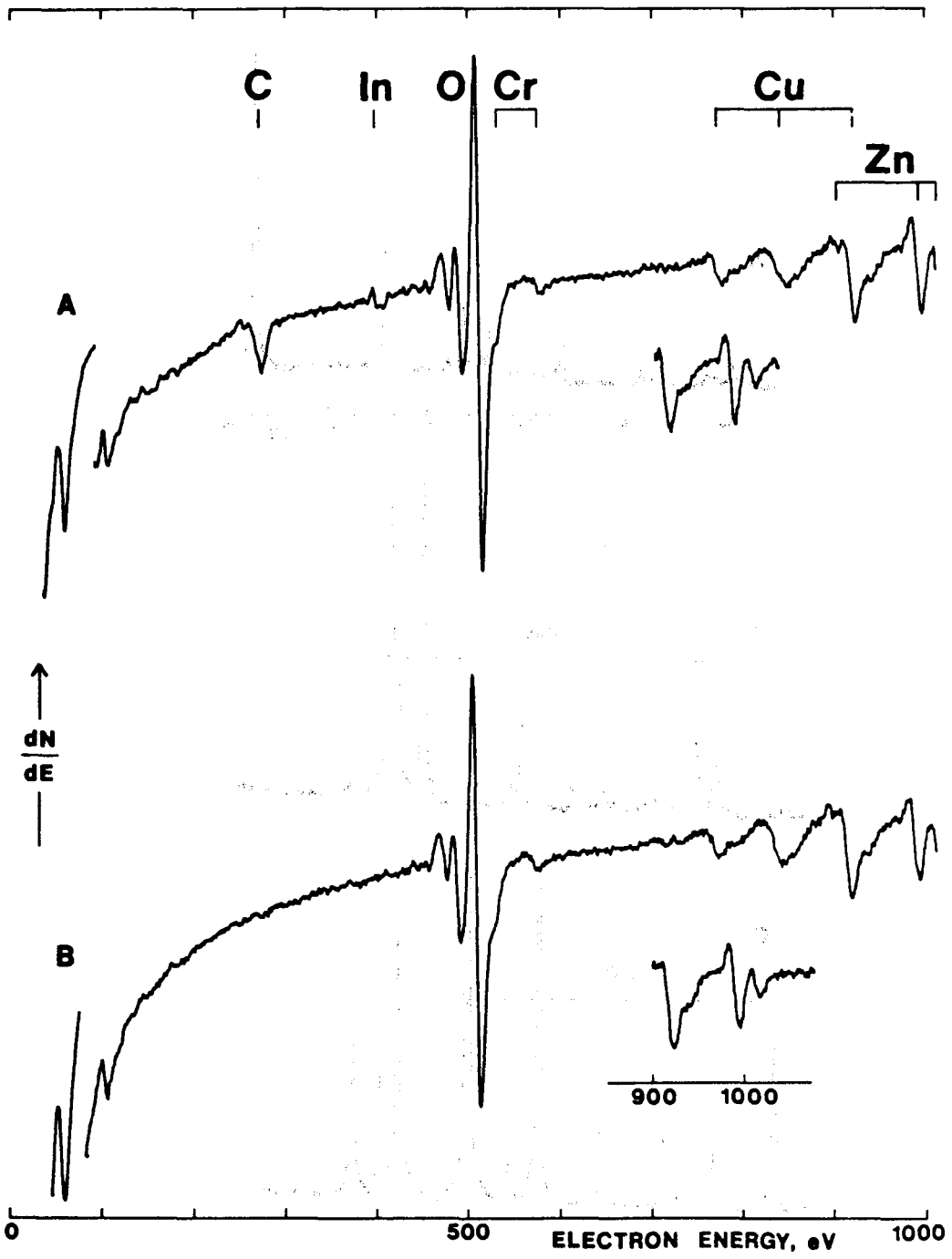

Figure 15. The Auger spectra of the Cu/Zn/Cr (60:30:10) catalyst (A) after calcination at 350°C and (B) after undergoing testing for methanol synthesis activity. Instrument settings: primary beam - 2000 eV at 60 MA; modulation - 5 eV.

ducing the CO_2 concentration in the reaction mixture.

Electronic Properties of Catalyst Components and of the Mixed Catalysts. Visual observations of the individual catalyst components and of the mixed catalysts indicated a profound mutual influence of the catalyst components in intimate contact upon each other's electronic spectra. For example, the reduced copper (pink)-zinc oxide (white) catalysts were black, despite the presence of only metallic copper and hexagonal zinc oxide phases identified by X-ray diffraction. To characterize the indicated electronic interactions in greater detail, near-infrared-visible-UV absorption spectra of pure components and the mixed catalysts were obtained. Figure 16 shows the electronic absorption spectra of (A) pure zinc oxide with its characteristic absorption edge at about 27,000 cm^{-1} [29], (B) metallic copper with the "d-hump" near 17,500 cm^{-1} [30] and (C) Cu_2O with its absorption edge around 16,500 cm^{-1} [31].

The spectra of the reduced Cu/ZnO catalysts are displayed in Figure 17 for the compositions (A) 5%, (B) 10%, (C) 30%, and (D) 67% copper. These spectra show, in addition to the spectral features of the pure components (i.e. the absorption edge of ZnO and the "d-hump" of metallic copper in the 30% and 67% Cu samples), a new near-infrared absorption with shoulder maxima at 4500 cm^{-1} and 14,000 cm^{-1} accompanied by an intense absorption continuum in the visible, which accounts for the black appearance of the mixed catalysts. The new absorption shoulders appear at frequencies substantially lower than those of the red Cu_2O (Figure 16C) and are present in all reduced Cu/ZnO, Cu/ZnO/Al_2O_3, and Cu/ZnO/Cr_2O_3 catalysts. A particular point of interest is the presence of this absorption in the single phase 5% Cu/ZnO sample in which ZnO is the only crystallographically identifiable phase. As metallic copper begins to nucleate in the 10% Cu/ZnO catalyst, X-ray diffraction shows weak copper lines and the "d-hump" begins to appear in the electronic spectrum (Figure 17B) but the infrared absorption continuum persists indicating that the major part of the copper is in the black ZnO. Upon further increase of copper concentration to 30% and 67%, both X-ray diffraction and electronic spectra provide evidence of a substantial amount of metallic copper;

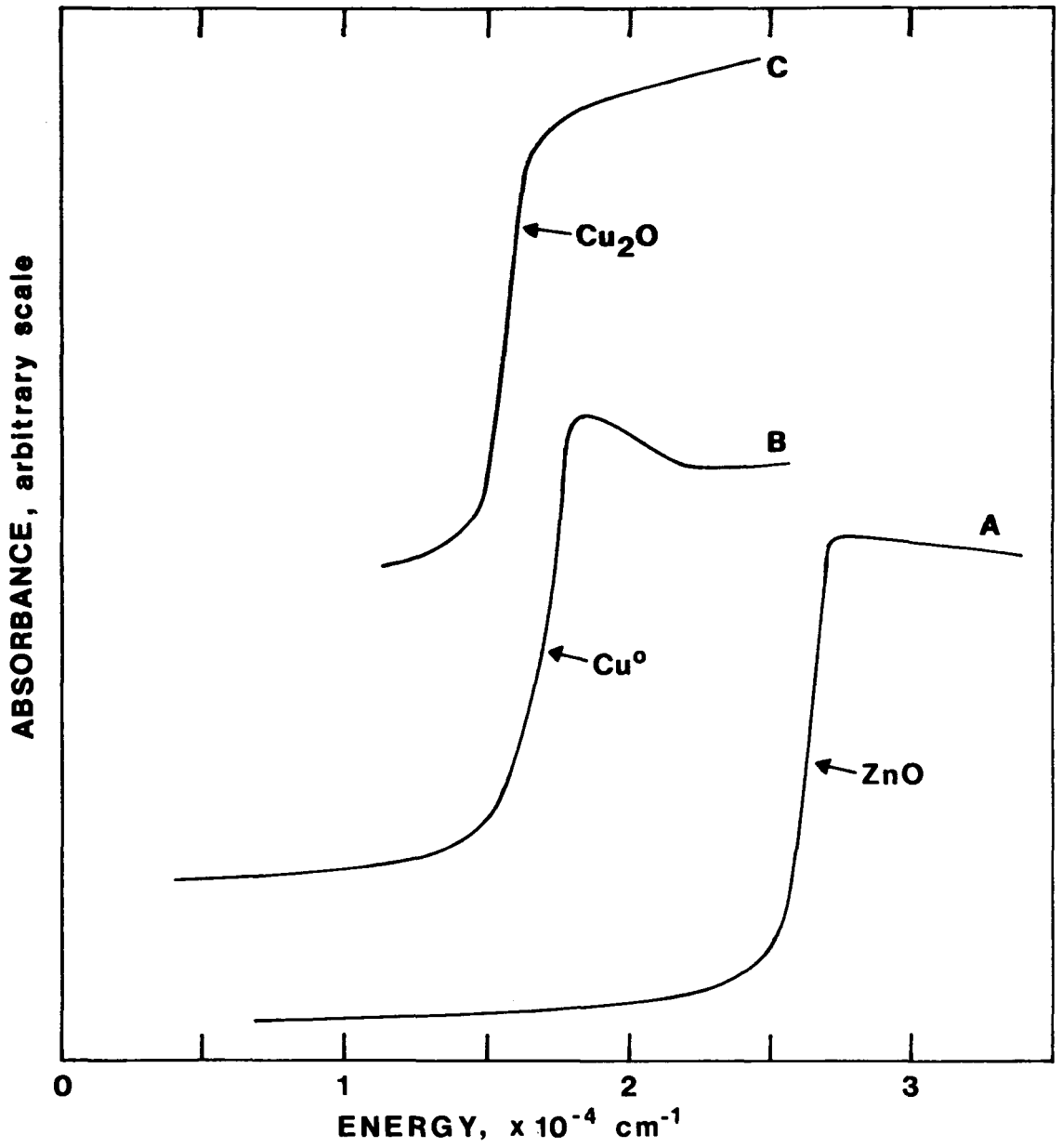

Figure 16. The diffuse reflectance spectra of (A) calcined zinc oxide, (B) metallic copper obtained by hydrogen reduction of copper(II) oxide, and (C) copper(I) oxide.

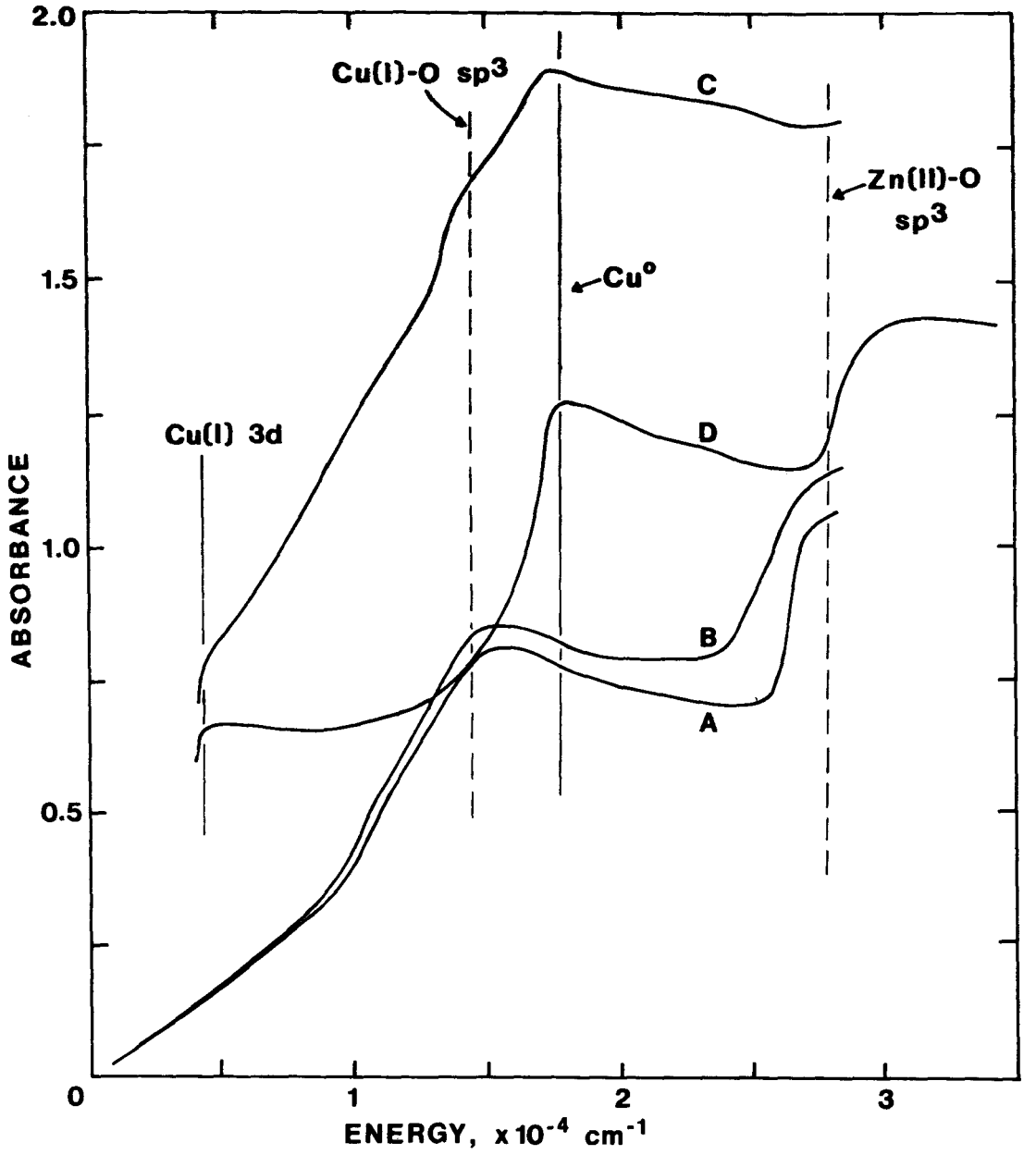

Figure 17. The diffuse reflectance spectra of reduced Cu/ZnO catalysts that initially contained (A) 5%, (B) 10%, (C) 30%, and (D) 67% CuO.

absorption shoulder becomes even more pronounced (Figures 17C, 17D).

Surface Areas and Pore Structures of the Cu/ZnO, Cu/ZnO/Al_2O_3, and Cu/ZnO/Cr_2O_3 Catalysts. The BET surface areas of the Cu/ZnO catalysts are given in Table 3.

TABLE 3
BET ARGON SURFACE AREAS OF THE Cu/ZnO CATALYSTS

CATALYST COMPOSITION (CuO/ZnO)	SURFACE AREA (m^2/g) Reduced	Used
0/100		25.2
2/98	43.1	28.9
10/90		27.0
20/80		30.0
30/70		37.1
40/60		13.5
50/50		10.3
67/33	6.3	8.6
100/0	1.5, 1.3	----

For comparison, the surface area of the Cu/ZnO/Al_2O_3 (60/30/10) catalyst tested in the present work was 33.4 m^2/g after use, while surface area of the Cu/ZnO/Cr_2O_3 (60/30/10) catalyst was 15.6 m^2/g after use. The comparable tested Cu/ZnO/Al_2O_3 catalyst that had been prepared from the acetates exhibited a final surface area of 26.1 m^2/g. The mesopore distributions of the Cu/ZnO, Cu/ZnO/Al_2O_3, and Cu/ZnO/Cr_2O_3 catalysts are displayed in Figure 18 along with the mesopore distribution of a commercial catalyst. The micropore volumes of these catalysts were found to be approximately the following: Cu/ZnO (67/33), 0.3 and 0.6; Cu/ZnO (30/70), 1.0; Cu/ZnO/Al_2O_3 (from acetates), 0.0; and Cu/ZnO/Cr_2O_3, 1.2 cm^3/g. The commercial catalyst had a micropore volume of about 3.0 cm^3/g at STP.

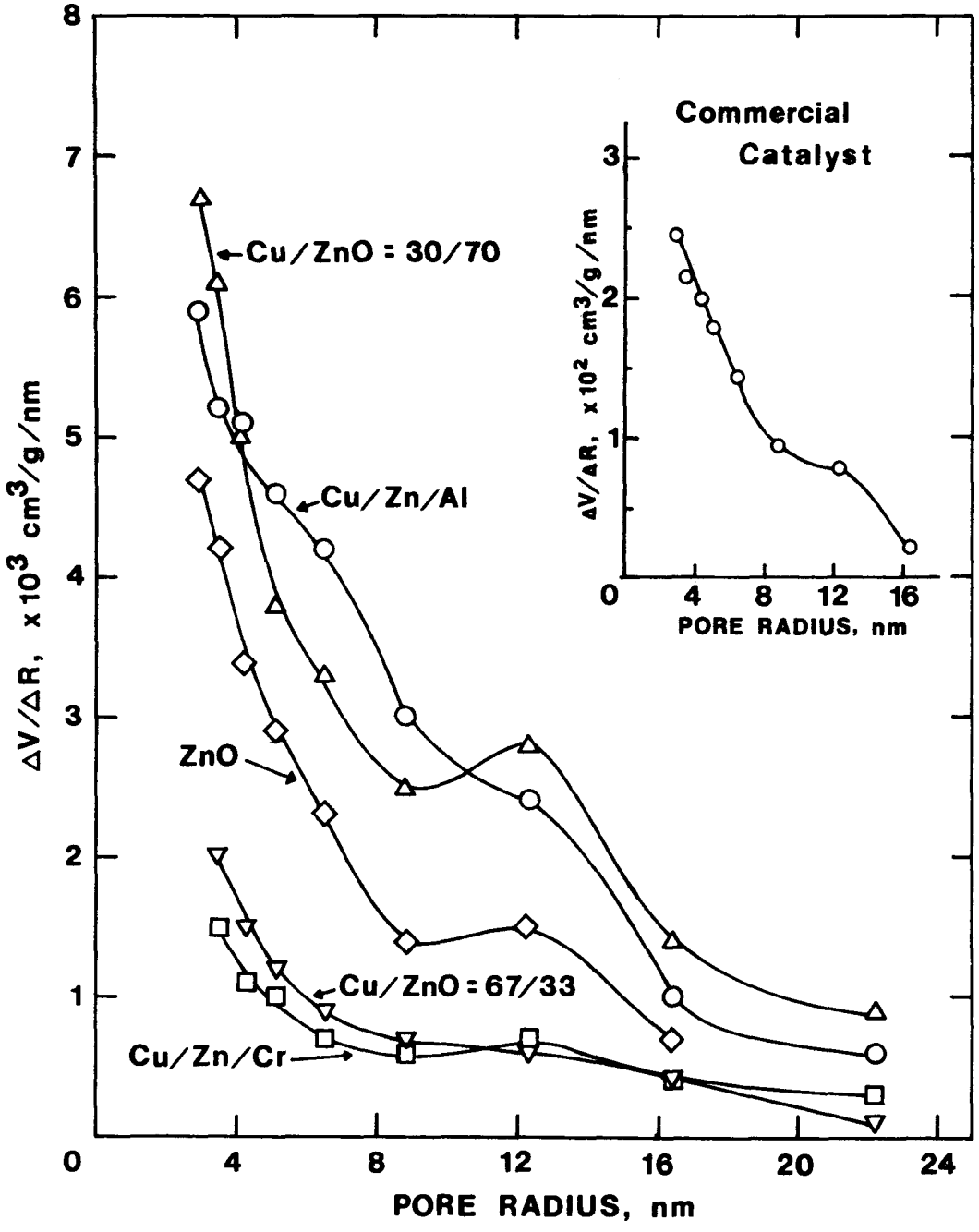

Figure 18. The mesopore volume distributions (cylindrical pores) for catalysts that had been tested for methanol synthesis activity.

Catalytic Activities of the Cu/ZnO, Cu/ZnO/Al_2O_3, and Cu/ZnO/Cr_2O_3 Catalysts in Methanol Synthesis. The catalyst testing was carried out in a flow reactor at a flow rate of 5000 GHSV with a $H_2/CO/CO_2$ = 70/24/6 mixture at 75 atm and in the temperature range 200-300°C. All catalysts investigated here were more than 99% selective to methanol with respect to carbon conversion. Under steady state conditions, carbon dioxide was not consumed but before steady state was reached, the CO_2 concentration sometimes temporarily decreased with concomitant formation of water.

The activities of the Cu/ZnO catalysts are compiled in Table 4 and compared in Figure 19 in terms of carbon conversion and methanol yields per gram of the catalyst as a function of catalyst composition. The table also contains the same activity date per unit total surface area of the catalyst. The activities at 250°C of pure ZnO and pure copper were zero within detection limits that were estimated to be less than 0.005 kg/l/hr in methanol yield. The activities of the Al_2O_3- and Cr_2O_3-based catalysts are given in Table 4, and it is evident that they are comparable to the activities of the binary Cu/ZnO catalysts. Side product analysis showed that no carbon containing products other than methanol were formed over the Cu/ZnO catalysts.

Discussion

The activity pattern of the Cu/ZnO system (Table 4) demonstrate that the active and selective low pressure methanol catalyst requires a simultaneous presence of copper and zinc oxide and that the effects of Al_2O_3 and Cr_2O_3 are secondary. Moreover, optical spectra of active catalysts show continuous absorption in the visible and near-infrared which disappears upon deactivation of the catalyst in a highly reducing mixture. For this reason, the genesis and electronic structure of the black active phase in the mixed catalysts is of prime interest for an explanation of the catalyst function and will be discussed first.

Catalyst Genesis and Electronic Structure. The precipitates in the Cu/Zn system, namely $Cu_2(OH)_3(NO_3$(I), $Zn_5(OH)_6(CO_3)_2$(II), and

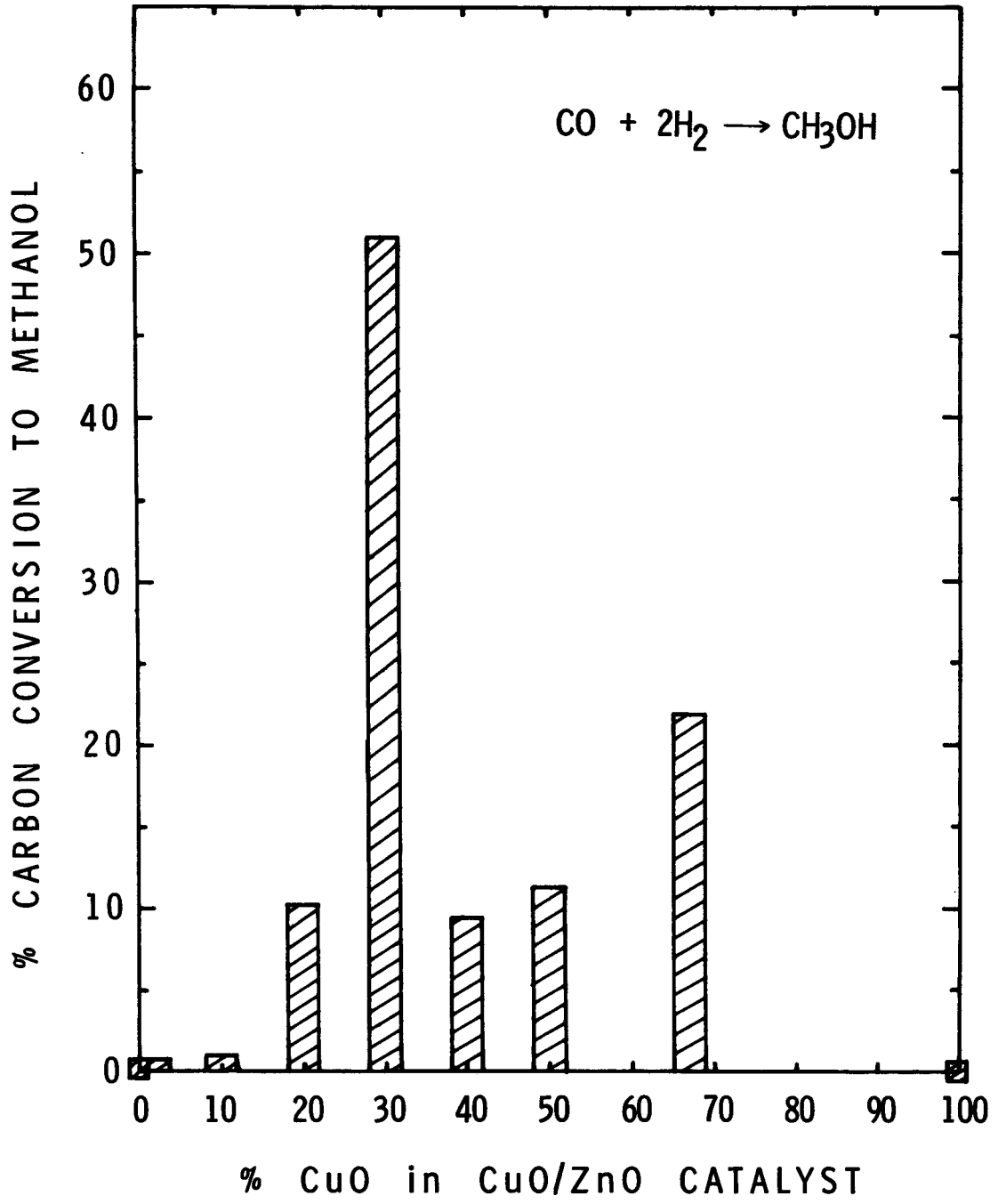

Figure 19. The methanol synthesis activity of the Cu/ZnO catalysts with a synthesis gas of $H_2/CO/CO_2$ = 70:24:6 vol % at 250°C, GHSV = 5000 Hr^{-1} and pressure of 75 atm.

TABLE 4

THE CATALYTIC TESTING RESULTS FOR THE Cu/ZnO SYSTEMS OBTAINED AT 250°C, 75 atm, AND GHSV + 5000 HR^{-1} WITH SYNGAS OF $H_2/CO/CO_2$ = 70/24/6 VOL %.

Catalyst Composition[a] $CuO/ZnO/M_2O_3$	Carbon Conversion	Yield kg/l/hr	Yield kg/kg/hr	Yield $kg/m^2/hr$ ($\times 10^5$)
0/100/0	0	0	0	0
2/98/0	0.7	0.02	0.03	0.10
10/90/0	1.0	0.02	0.02	0.70
20/80/0	10.2	0.22	0.24	0.80
30/70/0	51.1	1.10	1.35	3.63
40/60/0	9.6	0.21	0.18	1.33
50/50/0	11.3	0.25	0.20	1.94
67/33/0	21.8	0.48	0.41	4.76
100/0/0	0	0	0	0
60/30/10[b]	40.0	0.95	1.52	5.82
60/30/10[c]	17.0	0.45	0.58	1.73
60/30/10[d]	47.0	1.17	1.01	6.47

a) Weight percent as the oxides
b) M=Al, prepared from the acetates
c) M=Al, prepared from the nitrates, tested at 100 atm
d) M=Cr, tested at 100 atm

$(Cu/Zn)_2(OH)_2CO_3$(III) and their relative proportions did not influence the phase composition of the calcined CuO/ZnO or the reduced Cu/ZnO samples; however, they appeared to determine the catalyst dispersion and morphology by mechanisms that can be well understood from the structures of the compounds I, II, and III. It should first be noted that all three precipitates I, II, and III are thermodynamically more stable than simple hydroxides $Zn(OH)_2$, $Cu(OH)_2$, or carbonates of these two metals [32]. However, hydroxides may well be kinetic precursors of the hydroxycarbonates or hydroxynitrates as was indeed concluded by Vasserman and Silant'eva from their studies of the precipitation of compound I [33]. The sequence

of reactions based on the Vasserman-Silant'eva mechanism applied to our system is as follows:

$$CO_3^{2-} + H_2O \rightleftarrows HCO_3^- + OH^- \quad (3)$$

$$Cu(NO_3)_2 + 2OH^- \rightarrow Cu(OH)_{2(s)} + 2NO_3^- \quad (4)$$

$$3\ Cu(OH)_{2(s)} + Cu(NO_3)_2 \rightarrow \underset{(I)}{Cu(NO_3)_2 \cdot 3\ Cu(OH)_{2(s)}} \quad (5)$$

$$Zn(NO_3)_2 + 2OH^- \rightarrow Zn(OH)_{2(s)} + 2NO_3^- \quad (6)$$

$$2\ Zn(HCO_3)_2 + 3\ Zn(OH)_2 \rightarrow \underset{(II)}{Zn_5(OH)_6(CO_3)_{2(s)}} + H_2O + CO_2 \quad (7)$$

$$Zn(HCO_3)_2 + Cu(OH)_2 \rightarrow \underset{(III)}{CuZn(OH)_2\ CO_{3(s)}} + H_2O + CO_2 \quad (8)$$

As the precipitation occurred carbon dioxide was in fact released. Reactions (3) through (8) may be used to explain the compositions of the precipitates at various Cu/Zn ratios (Figure 12). With increasing Cu/Zn ratio, the relative amount of the zinc hydroxycarbonate (II) continuously decreases, indicating an independent precipitation mechanism (equations (6) and (7)). Simultaneously, the amount of the two copper compounds (I) and (III) increases so that in the range where zinc concentrations are large (Cu/Zn = 0.1 to 0.5) the mixed copper zinc hydroxycarbonate (III) is preferred, whereas at large copper concentrations the copper hydroxynitrate (II) is preferred. Compound III provides for the most intimate mixture of copper and zinc and is known as the mineral rosalite with Cu/Zn ratios varying from 1.4 to 1.8 [34].

Upon stepwise calcination to 350°C, all three compounds I, II, and III decompose to oxides MO where M is zinc or copper. Compound II gives rise to zinc oxide, compound III to mixed zinc oxide and cupric oxide, and compound I to cupric oxide. Possibly some copper may be substituted for zinc in compound II and zinc for copper in compound I but the whole precipitation pattern shows a clear

preference of zinc for II and copper for I. The structure of the mixed copper zinc hydroxycarbonate III (Figure 20) is such that each metal atom is in square planar or near square planar coordination of oxygen atoms belonging to the OH^- and $CO_3^=$ groups. Its decomposition may be visualized as a reaction of each $CO_3^=$ group with two protons from the nearest OH^- groups followed by the release of $H_2O + CO_2$ along channels parallel to the c axis, leaving behind an open network of Cu and Zn atoms square planarly and linearly coordinated to the O atoms originating from the OH^- groups. This network is structurally related to the tetragonal CuO [18] but not to the hexagonal ZnO [19]. Since ZnO and CuO have to segregate because of their different crystal structures and limited solubilities, the (Cu,Zn) oxide network generated by the decomposition of compound III will initially separate into a very fine interdispersion of ZnO and CuO with highly imperfect ZnO. This is indeed confirmed by X-ray line broadening and electron microscopy of the 30% Cu catalyst [27] which originates from the precipitate having maximum concentration of compound III. On the other hand, at concentrations of 40% copper and higher the ZnO crystallites formed during calcination are well-developed into hexagonal platelets [27]. The platelet morphology coincides with the presence of compound I in the catalyst precursor, indicating that an epitaxial mechanism may be operating in determining the ZnO morphology. Indeed, compound I has pseudohexagonal stable planes (001) of the structure shown in Figure 21. That these are surface planes is corroborated by the XPS analysis in which the nitrogen peak corresponding to the hidden nitrate groups is very small compared to those of copper and oxygen. Also drawn to scale in Figure 21 is the triequiangular net of zinc atoms in the basal (0001) plane of ZnO, demonstrating that zinc oxide may epitaxially grow on copper hydroxynitrate I with its basal plane including the major growth directions. The explanation of hexagonal platelet morphology of ZnO at Cu concentrations equal to or greater than 40% presently proposed is based upon a greater thermodynamic stability of copper hydroxynitrate I than that of the carbonates II and III [35]: as the carbonates II and III decompose during the stepwise calcination, the undecomposed $Cu_2(OH)_3NO_3$ acts as a seed for crystallization of the nascent ZnO, which is forced to grow as hexagonal platelets

rather than as its normal needle-like habit. In the latter stages of calcination, $Cu_2(OH)_3NO_3$ decomposes into a separate phase of CuO, leaving the ZnO crystallites unchanged. The ZnO morphology is also retained after reduction in which Cu metal is produced from CuO in the mixed samples. Thus, the composition of the precipitates determines the crystal shape and dispersion of ZnO in the final catalyst.

It has already been noted in the Results section that the ZnO crystallites contain, after calcination, 2-4% of dissolved CuO at nominal compositions between 15% and 50% CuO. The amount of copper dissolved in ZnO after reduction was even larger, up to 12% in the Cu/ZnO catalysts and up to 14% in the $Cu/ZnO/Al_2O_3$ or Cr_2O_3 catalysts [27]. At the same time, optical measurements revealed a new black compound with a spectrum unlike that of Cu metal, Cu^{++} ions in ZnO [36], or Cu_2O. This new spectrum is assigned to Cu^{1+} species dissolved in ZnO as there remains no other possibility consistent with all of the experimental observations reported here. The dissolution of Cu^{1+} in ZnO is certainly favored by the fact that Cu^{1+} is isoelectronic with Zn^{2+} and that is assumes, like Zn^{2+}, a tetrahedral coordination in a number of its inorganic compounds. The limitation of Cu^{1+} dissolution in ZnO consists in the requirement of electroneutrality upon substitution of some Zn^{2+} by Cu^{1+}, which must be ensured either by oxygen vacancies or by interstitial zinc. It is tentatively suggested that the solubility limit, 12% of Cu^{1+}, is determined by the number of oxygen vacancies, 6%, that the ZnO crystal can accomodate without loss of crystallinity. Further increase of Cu^{1+} concentration may be obtained if trivalent ions are simultaneously dissolved in ZnO, since the $Cu^{1+} - M^{3+}$ pairs substitute for $Zn^{2+} - Zn^{2+}$ pairs without increasing the number of oxygen vacancies.

Absorption spectra of the Cu/ZnO catalysts confirm that the new electronic states are created in this system with an absorption edge below those of ZnO, Cu metal, and Cu_2O, and parallel diffraction studies show that ZnO is the host lattice to these new electronic states. At the same time, the band edge of ZnO is preserved, or only slightly shifted indicating that the new electronic states

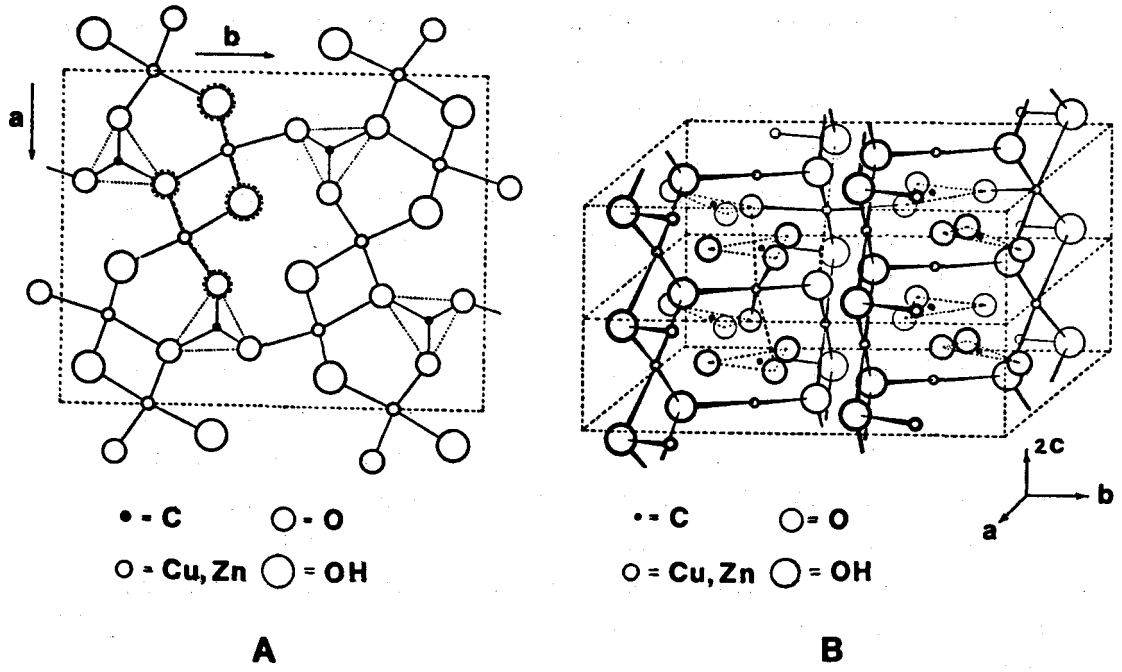

Figure 20. Representations of the crystal structure of rosalite (A) projected on the (001) plane and (B) showing the spatial relationships of two unit cells.

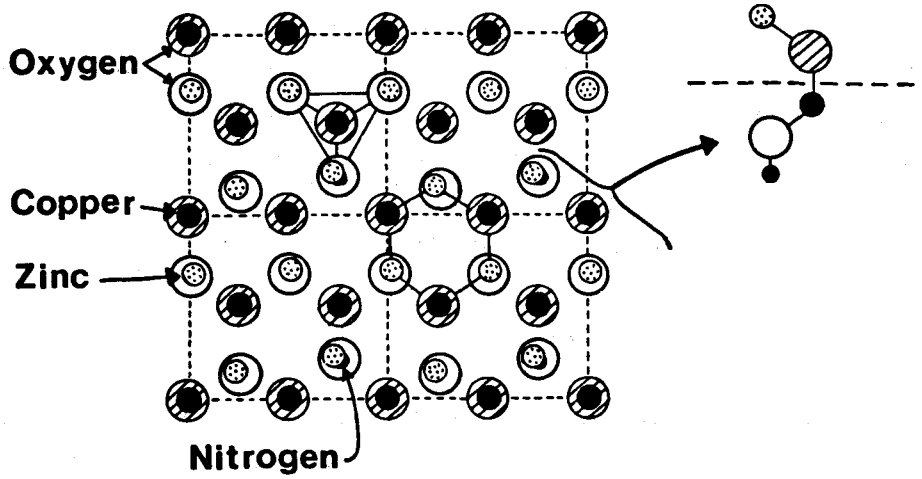

Figure 21. A representation of the surface structure (001) of $Cu_2(OH)_3NO_3$ that has a layer of exposed copper atoms on which hexagonal ZnO can easily crystallize along directions in the basal plane.

are located in the forbidden band of ZnO. Such an electronic spectrum is entirely expected upon substitution of some Zn^{2+} in the zinc oxide lattice by Cu^{1+} as illustrated in Figure 22. The origin of the band spectrum of ZnO from atomic Zn 4s, O 2p, and Zn 3d levels is shown in Figure 22A so that the atomic levels, the experimental bandgap of 0.24 Ry (3.3 eV) [37], and the theoretical bandwidths of the valence and the Zn 3d band [38-40] are drawn to scale. In contrast to the Zn 3d band, which lies below the valence band of zinc oxide because the Zn 3d atomic levels are below the O 2p levels, the Cu 3d band is expected to be located above the valence band of the zinc oxide because the Cu 3d levels are located well above O 2p and are, in fact, as high as the Zn 4s levels. In addition, the Cu 4s level will give rise to band edges similar to the Zn 4s level, but located higher in the energy scale with the valence band maximum in the bandgap of ZnO. On the basis of the energy levels discussed above, there are two possible sets of new levels in the Cu^{1+}/ZnO solution: the filled 3d band of copper and the sp^3 valence band originating from Cu 4s and O 2p atomic levels. The bandwidth of the Cu 3d band will depend on the copper concentration since it is determined by Cu 3d-Cu 3d overlap; the bandwidth of the sp^3 Cu-O valence band is expected to be independent of copper concentration since it depends primarily only on the energy difference of the Cu 4s and O 2p atomic levels [41].

In view of the above model, the absorption spectra in Figure 17 indicate that the new electronic states in Cu/ZnO have a considerable Cu 3d character. There is a significant shift to lower energies of the absorption edge in the near-infrared between the 5% or 10% Cu/ZnO samples and the 67% Cu/ZnO catalyst, which reflects the increase of the copper concentration in ZnO from subsaturation in the two low copper samples to saturation in the high copper sample.

A note should be added on the possible role of interstitial zinc and oxygen vacancies in the absorption spectra. Zinc oxide with excess zinc displays a weak absorption in the blue region [42] and oxygen vacancies in copper-containing oxides give rise to luminescence and weak absorption in the visible and near-infrared [31]. Neither of these features could account for the near-infrared absorption continuum and its intensity, and thus interstitial zinc

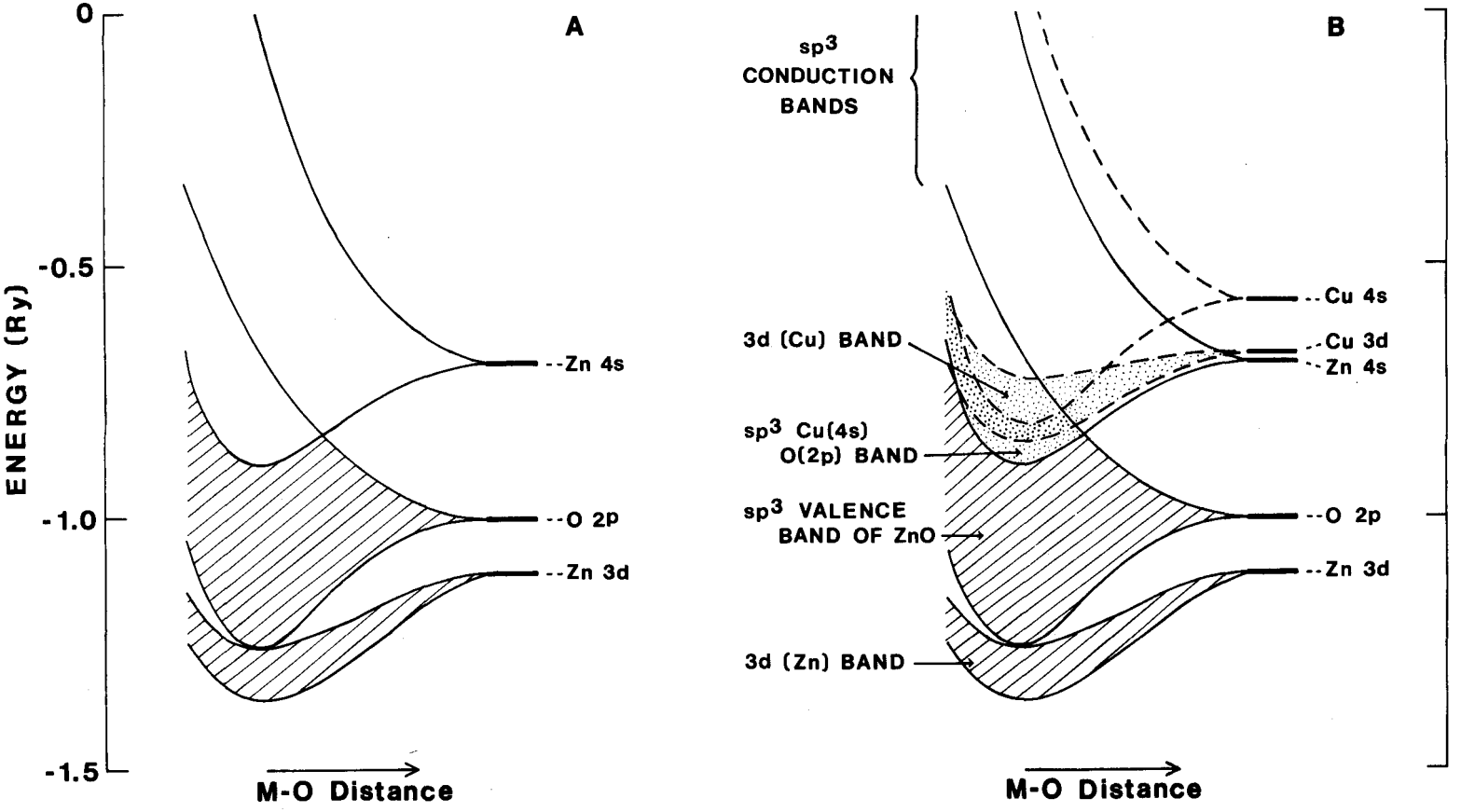

Figure 22. A diagram showing the band spectra of (A) ZnO and (B) Cu(I)/ZnO solid solution.

and oxygen vacancies may give rise at most to secondary spectral features superimposed on the fundamental band spectrum of the Cu^{1+}/ZnO solution discussed above. A separate experiment confirmed that the reduction and reaction conditions employed in methanol synthesis are not sufficient to produce a visibly detectable color change in pure zinc oxide, leaving this compound white after exposure to 2% H_2/98% N_2 at 250°C for 4 hr and to the $H_2/CO/CO_2$ mixture at 75 atm up to 320°C for 10 hr.

Activity Pattern of the Copper-Zinc Oxide Containing Catalysts and the Synthesis Mechanism. The results of catalytic testing of the Cu/ZnO, Cu/ZnO/Al_2O_3 and Cu/ZnO/Cr_2O_3 catalysts clearly establish that the Cu/ZnO catalysts have an activity toward methanol synthesis comparable per weight and per unit surface area to that of the Cu/ZnO/Al_2O_3 and Cu/ZnO/Cr_2O_3 catalysts. Also, the selectivity of the Cu/ZnO catalysts is equal to or exceeds that of the alumina or chromia based catalysts. No special pore distribution is necessary for highly effective Cu/ZnO catalyst with or without alumina and chromia, and thus the synthesis appears to proceed as a surface reaction without diffusion control.

The mutual promotion effect of copper and zinc oxide is illustrated by the activity pattern in Table 4 and in Figure 19, which shows that a substantial activity is displayed by the various intermediate Cu/ZnO compositions while the pure components, i.e. copper metal and zinc oxide, are inactive under the low-pressure regime. Since no new phase other than normal crystal structures of Cu metal and zinc oxide exists in the mixed Cu/ZnO catalysts, the promotion effect can only stem from the catalytic activity of a solid solution such as the Cu^{1+}/ZnO system described in the previous paragraph, from uncommon crystal planes and surface imperfections stabilized by the presence of the second phase, and from long range effects resulting from electron transfer between the active and support phases. In this report we shall discuss only the dominant effect which is associated with the new electronic structure of the Cu^{1+}/ZnO solution. The effects of crystal morphology will be reported in detail elsewhere [27]. It is only noted here that both principal ZnO morphologies, the rod-like network bounded by

prism planes predominant at 2%-30% Cu/ZnO and the hexagonal platelets bounded by the basal planes occurring at 40-67% Cu/ZnO, are catalytically active and selective to methanol. The rod-like networks have a higher surface area and hence a higher activity than the platelets, provided that enough Cu^{1+} is dissolved in the zinc oxide. Considerations of long range electron transfer in small crystallites in contact with supporting phase, although conceptually developed [43], give rise to estimates of only marginal effects on the surface equilibria in the present systems, and will be reported elsewhere in conjunction with a wider range of supports.

The mechanism of the catalytic function of the Cu^{+}/ZnO solution proposed here is based on the known properties of zinc oxide and univalent copper. Zinc oxide is a good hydrogenation catalyst [44] that activates hydrogen by heteropolar splitting giving rise to ZnH and OH groups on the ZnO surface [45]. However, the chemisorption activity of ZnO toward CO is poor [46], evidently because of unavailability of the deeply lying Zn 3d orbitals for back-donation. The behavior of Cu^{+} in various low coordinated compounds and surfaces is just the opposite: certain Cu^{+} compounds quantitatively adsorb carbon monoxide in solutions [47] and Cu^{+} ions in zeolites form 1:1 complexes with carbon monoxide [48] while they do not absorb hydrogen up to 100-150°C [49]. The binding of CO by Cu^{+} can be easily understood from the high energy and spatial extent of the unscreened Cu 3d orbitals available for backbonding into the π^* orbitals of CO [50]. Similar CO bonding is proposed here for the Cu^{+} centers in ZnO: the Cu 3d orbitals are now broadened into a band as indicated in Figure 22, but they are still the highest occupied orbitals suited for backbonding into the π^* orbitals of CO.

The initial step of methanol synthesis over the Cu^{+}/ZnO catalyst is thus proposed to be chemisorption and activation of CO on the Cu^{+} centers and of hydrogen on the surrounding ZnO surface. The hydrogenation of CO may proceed in a series of subsequent steps, one of which must effect hydrogenation of the oxygen end of CO and another the hydrogenolysis of the Cu-C bond. A possible complete mechanism involving formyl and hydroxycarbene intermediates is

illustrated on the next page.

The heteropolar splitting of hydrogen and the binding of CO to cationic Cu^+ centers imposes electrophilic attack of the carbon end of CO by protons and nucleophilic attack of the oxygen end of CO by hydride ions, if the complex process involving the electron equilibria in the semiconductor surface can be expressed in the simplified language of mechanistic chemistry of organic molecules. As a limiting step is proposed the hydrogenolysis of the $Cu\text{-}CH_2OH$ bond in view of earlier reports that a CH_3O composition persists on the catalyst surface exposed to H_2:CO mixtures ranging from 1:20 to 100:1 [51].

Effects of Poisons and Oxidizing Gases on the Synthesis. The sensitivity of copper containing methanol synthesis catalysts to poisoning by sulfur has been known for a long time, and, in fact, Natta rejected the copper-containing catalysts as impractical because of their rapid deactivation in the presence of hydrogen sulfide [52]. He attributed the sulfur poisoning to the formation of bulk CuS according to reaction (9).

$$Cu + H_2S = CuS + H_2 \quad K_{550°K} = 3.2 \tag{9}$$

Another bulk sulfide might be formed by reaction (10)

$$2Cu + H_2S = Cu_2S + H_2 \quad K_{550°K} = 3.32 \times 10^4 \tag{10}$$

However, it was later found that the copper-containing catalysts were poisoned by levels of H_2S as low as 0.1 ppm [53], an effect that cannot be accounted for either by reaction (9) or by (10). Reaction (9), because of its small equilibrium constant, does not come into consideration for sulfide formation until the H_2S concentration in hydrogen reaches 24%, and reaction (10) has equilibrium shifted to the right cnly at more than 30 ppm H_2S, while the catalysts are severely poisoned at substantially lower levels.

According to the presently proposed synthesis mechanism, the active catalyst is a zinc oxide phase with dissolved Cu^+ species, and a

Zn
Cu
Zn
O
H
C

simple surface poisoning reaction may be suggested in which no hydrogen is produced and therefore a substantially greater driving force than in reactions (9) and (10) exists for the formation of the right-hand side products of reaction (11).

$$Cu^+ + O^{2-} + H_2S = Cu^+SH^- + OH^- \qquad (11)$$

Similarly, halogen poisoning, e.g. by hydrogen chloride [54], may initially proceed as a surface reaction giving rise to Cu^+Cl^- and OH^- species. This might be followed by escape of the volatile cuprous chloride into the gas phase and an irreversible removal of the Cu^+ centers from the catalyst.

In contrast to the poisoning by sulfur and halogen containing gases, methanol yields were enhanced by the presence of carbon dioxide, water, and oxygen. Both oxygen and water increased the yields more than an equivalent amount of carbon dioxide [55], and upon pulsed additions of oxygen to the CO/H_2 feed gas, up to a fifteen-fold increase of methanol yields could be obtained [56]. An additional observation of interest was made in the present work: in the absence of CO_2 (or H_2O and O_2), the catalyst gradually lost activity with concomitant change of color from black to pink with no carbon deposition and very little change in surface area. The physical changes accompanying the catalyst deactivation indicated that the active Cu^+/ZnO phase was reduced to inactive copper metal by the reaction mixture CO/H_2. In view of this mechanism of deactivation, the rate enhancing effect of oxygen, water, and carbon dioxide is to decrease the reduction potential of the CO/H_2 feed gas and to keep Cu^+ in the active Cu^+/ZnO state. It should be noted that the virtual oxygen pressures for the CO_2/CO and H_2O/H_2 ratios frequently employed in the synthesis are sufficient for oxidizing fine copper dispersions but not bulk copper metal [57] so that the reduction-deactivation mechanism is irreversible once large crystallites of copper metal are produced from the Cu^+/ZnO phase.

Summary

The catalytic activity of the low pressure $Cu/ZnO/Al_2O_3$ catalysts for methanol synthesis resides in the Cu/ZnO system. No special

pore distribution or presence of crystalline phases such as spinels is necessary for selectivity to methanol. The Cu/ZnO system stabilizes a black substance which has been identified as a Cu^+ solution in ZnO.

A synthesis mechanism is proposed whereby the Cu^+ centers chemisorb and activate carbon monoxide and the ZnO surface activates hydrogen. Catalyst deactivation in the CO/H_2 mixture is explained as the reduction of Cu^+ to inactive copper metal, and the promotion effect of O_2, H_2O, and CO_2 as a maintenance of oxidation potential high enough to keep the copper in the active Cu^+ state. Poisoning by hydrogen sulfide and HCl is attributed to irreversible heteropolar chemisorption of H_2S and HCl with blocking of the Cu^+ centers by the SH^- and Cl^- groups.

C. TASK 3: SINGLE PHASE CATALYSTS

A low level effort was extended in the area of preparation of single phase oxide catalysts. This entailed trying to prepare pure solid solutions with zinc oxide as the major component. It was found that this task overlapped with Task 2, and therefore some of the results have already been presented in the preceeding portion of this report.

Samples corresponding to 2:98, 5:95, and 10:90 were prepared by coprecipitation, dried, and calcined to 350°C as previously described. The colors of the calcined samples extended from light gray (2:98) to brownish gray to brown. Portions of these samples were heated to 900°C in air in 50°C-30 increments and then equilibrated at 900°C for 17 hr. The 2:98 solid became bright yellow while the 10:90 sample was a uniform light black color. The 5:95 catalyst appeared to be a drab green. However, close inspection showed that this sample was a mixture of yellow particles and light black particles. The yellow color of the 2:98 catalyst indicated that a solid solution of Cu^{2+} in ZnO was achieved at 900°C, where the divalent copper ions are held in sites of tetrahedral geometry. However, the color of the catalyst calcined to 350°C might indicate that most of the copper existed as CuO in a separate phase, but this phase could not be detected by X-ray powder diffraction.

Samples corresponding to 5:95 and 10:90, prepared by manual mixing of pure CuO with ZnO in the calculated proportions, did not yield yellow products upon calcination at 900°C for 48 hr. However, a 2:98 catalyst prepared and treated in the same way did produce a yellow solid solution.

Reduction studies were carried out on the coprecipitated samples using the same techniques as were described in the previous sections

of this report. Using a large heater around the vertical reduction apparatus and a slow heating rate, a 20 hr reduction using 2% H_2-98% N_2 yielded samples varying in color from light gray (2:98) to dark gray. Repeating the reductions with a smaller heater and fresh samples, the products were uniformly black, in agreement with the 20:80 and 30:70 catalysts.

Beginning with a pelletized portion of the coprecipitated, calcined catalyst, a methanol synthesis test was made. A small activity was noted, which increased with temperature as expected; at temperatures of 250, 275, and 290°C, the % carbon conversions were 0.68, 2.14, and 3.74, respectively. The used catalyst was light black, but upon standing in air for a few months it became a uniform gray color. A catalytic testing of the yellow solid solution has not been carried out.

These results corroborate other data [36] that suggest that Cu^{2+} will form a solid solution with ZnO to an extent of only 2-3%. Upon reduction, samples richer in copper can form greater concentrations of solid solutions with copper in the monovalent state, plus fine dispersions of metallic copper. Although a systematic study has not yet been done, it appears that air can reoxidize at least part of the reduced copper at ambient temperature to form CuO.

D. TASK 4: POISONING OF TERTIARY METHANOL SYNTHESIS CATALYSTS

Only a preliminary poisoning experiment has been carried out since the research projects under Task 1 and 2 were expanded and intensively pursued. A Cu/Zn/Cr oxide catalyst (60:30:10) was reduced and tested for methanol synthesis using the usual procedures and conditions, except that a pressure of 100 atm was used instead of 75 atm. At 250°C, the catalytic activity was gradually decreasing until a trace of COS was added to the synthesis gas stream. A subsequent increase in catalytic activity was noted.

The apparent reactivation of the catalyst by COS suggests that the mechanism of interaction of this impurity with the catalyst might be entirely different from the mechanism of interaction of H_2S with the catalyst. Hydrogen sulfide is a reducing gas that strongly interacts with the catalyst and deposits sulfur on the catalyst as sulfide. On the other hand, COS might act as an oxidant toward the catalyst. Therefore, further experimentation using COS as a minor component of the synthesis gas, with and without the presence of CO_2, is desirable.

IV. CONCLUSIONS

The catalysts from Chem Systems were characterized with the aim of discerning differences between the sets of reference, used and active, used but deactivated, and poisoned catalysts. The poisoned catalysts contained large amounts of sulfur or chlorine, which were used as the poisoning agents. These latter catalysts had also suffered an appreciable loss of surface area, as shown by Argon adsorption measurements. However, the deactivated catalysts showed little decrease in surface area and little surface contamination. All analytical measurements could be routinely carried out on the catalysts used in the liquid phase methanol synthesis testing because a successful method of removing the white oil was developed during this project.

The cause or causes of deactivation for the two used deactivated, but unpoisoned, catalysts were not established. Possible reasons for this include the following:

1. the small samples received at Lehigh University were not representative of the deactivated catalyst charges,
2. the solvent extraction procedure used to remove the white oil also removed the species that caused the deactivation,
3. the mechanism of deactivation is different from surface area changes and from bulk compositional changes, or
4. the composition of the synthesis gas was such that the concentration of reactive species (sites) on the surface of the catalyst was gradually reduced.

Additional insight into the mechanism of deactivation was achieved by studying the binary Cu/ZnO catalysts. It was established that the loss of surface area is not, of itself, the major contributing factor in deactivation. The surface areas of the binary Cu/ZnO catalysts were appreciably lower than those of the tertiary catalysts, yet the percent carbon conversions to methanol were comparable. It appears that much of the surface area of tertiary

catalysts is due to the Al_2O_3 or Cr_2O_3, which is added as a support. It has now been demonstrated that this third component is not necessary for methanol synthesis. In connection with this, the absence of Al_2O_3 and Cr_2O_3 in the binary catalyst systems makes the hypothesis, proposed by others, that the catalytically active species is a spinel, invalid.

In consideration of the data contained herein, a mechanistic scheme for methanol formation is presented. Hydrogen is dissociatively activated on the ZnO surface. It is proposed that CO is adsorbed on adjacent sites that consist of Cu^+ ions in solid solution with zinc oxide. The presence of CO_2 in the synthesis gas produces enough oxidizing power to maintain a "sufficient" quantity of active Cu^+ sites for methanol synthesis to occur in a constant yield. It now appears that COS might behave in a similar manner, but additional experimentation is required to verify this. Poisoning of these copper-based catalysts by H_2S and CH_3Cl could initially consist of a simple surface poisoning reaction analogous to complex formation. In the alumina-based tertiary catalysts, there appears to be a loss of aluminum associated with chlorine poisoning that occurs by volatilization of aluminum chloride. Although this would result in a decrease of surface area, it is not clear whether this would cause deactivation.

The most likely deactivation mechanism is believed to be over-reduction of the catalyst, prior to or during the course of synthesis with a concomitant loss of the active Cu^+/ZnO species into the inactive copper metal phase.

V. REFERENCES AND NOTES

1. "National Energy Outlook," Federal Energy Administration, Washington, D.C., 1976, p. 5.
2. Chem. Eng. News, Jan. 31, 1977, p. 17.
3. Chem. Eng. News, Dec. 20, 1976, p. 8.
4. T. A. Hendrickson in "Synthetic Fuels Data Handbook,: Cameron Engineers, Inc., Denver, 1975, pp. 204-205.
5. Hydrocarbon Processing, April 1973, p. 17.
6. Environmental Sci. Tech., Nov. 1973, p. 1002.
7. R. W. Duhl, "Methyl Fuel from Remote Gas Sources," Engineering Foundation Conference on Methanol as an Alternate Fuel, July 1974.
8. P. M. Jarvis, "Methanol as Gas Turbine Fuel," Engineering Foundation Conference on Methanol as an Alternate Fuel, July 1974.
9. R. Williams, "Methanol - The Energy Chemical," a proposed study, Technical & Economic Services, Inc., and The Charles A. Stokes Consulting Group, Princeton, N.J., 1976.
10. Automotive Engineering, 85, Dec. 1977, p. 51.
11. The Federal Register, 37, No. 22140, Oct. 18, 1972.
12. Wilks Scientific Corporation, "OSHA Concentration Limits for Gases" table, 1975.
13. For example, see "Liquid Phase Methanol," Annual Report submitted by Chem Systems, Inc., New York to the Electric Power Research Institute, Project 317, EPRI AF-202, Aug. 1976.
14. S. Brunauer, R. Sh. Mikhoil, and E. E. Bodor, J. Colloid Interface Sci., 24, 451 (1967); E. E. Bodor, I. Odler, and J. Skalny, J. Colloid Interface Sci., 32, 367 (1970).
15. K. S. W. Sing, "Surface Area Determination," IUPAC Symp. Proceedings, Bristol, U. K., 1969.
16. "Handbook of Chemistry and Physics," 50th Ed., ed. by R. C. Weast, The Chemical Rubber Co., Cleveland, Ohio, 1970, p. B-83.
17. These estimates were made on the basis of an activation energy of 30 kcal/mol (e.g. see G. Natta in "Catalysis," Vol. III, P. H. Emmett, Ed., Reinhold Publ. Corp., N.Y., 1955) and the observation of comparable activities of pure ZnO at 350 atm and 400°C and Cu/ZnO at 75 atm and 250°C. Metallic copper has less catalytic activity than did ZnO.

18. G. Tunell, E. Posnjak, and C. J. Ksanda, Z. Krist., A90, 120 (1935); tenorite CuO.

19. C. W. Bunn, Proc. Phy. Soc. London, 47, 835 (1935).

20. "Powder Diffraction File Search Manual-Inorganic (Fink Method)," Joint Committee on Powder Diffraction Standards, Swarthmore, Pennsylvania, 1973.

21. "International Tables for X-ray Crystallography," Vol. 3, K. Lonsdale et al., Ed., The Keynock Press, Birmingham, England, 1954.

22. B. D. Cullity, "Elements of X-ray Diffraction," Addison Wesley Publ. Co., Reading, Mass., 1956.

23. K. Klier, Catal. Rev., 1, 207 (1967).

24. W. Nowacki and R. Scheideggar, Helv. Chim. Acta, 35, 375 (1952).

25. S. Ghose, Acta Crystallogr., 17, 1051 (1964).

26. Compound III is isomorphous with malachite, $Cu_2(OH)_2CO_3$, the structure of which is known [A. F. Wells, Acta Crystallogr., 4, 200 (1951)].

27. Part II of this communication, which deals with the electron microscopy studies, will be published elsewhere.

28. This assignment is based upon the relative abundances of copper hydroxynitrate and copper or zinc hydroxycarbonates. It is not possible to make assignments on the basis of literature reporting XPS energies of O(1s) in reference compounds because the published values for the same compound differ by up to 3 eV, viz. N. S. McIntyre and M. G. Cook, Anal. Chem., 47, 2208 (1975) and D. C. Frost, A. Ishitani, and C. A. McDowell, Molecular Physics, 24, 861 (1972).

29. E. Scharowsky, Z. Physik, 135, 318 (1953).

30. S. Roberts, Phys. Rev., 118, 1509 (1960); D. Beaglehole, Proc. Phys. Soc. (London), 85, 1007 (1965).

31. J. Bloem, Philips Res. Rept., 13, 167 (1958).

32. F. D. Rossini, D. D. Wagman, W. H. Evans, S. Levine, and I. Jaffe, "Selected Values of Chemical Thermodynamic Properties," National Bureau of Standards Circular #500, 1952.

33. I. M. Vasserman and N. I. Silant'eva, Russ. J. Inorg. Chem., 13, 1041 (1968).

34. S. D. H. Donnay and H. M. Ondik, "Crystal Data: Determinative Tables," Vol. 2, National Bureau of Standards, Washington, D. C. 1973.

35. The enthalpy of decomposition of $Cu_2(OH)_3NO_3$ to CuO, H_2O, NO_2 and O_2 is 23 kcal/mol of copper, while that of $Cu(OH)_2$ is 12 kcal/mol, $CuCO_3$ is 11 kcal/mol, $Zn(OH)_2$ is 12.5 kcal/mol, and $ZnCO_3$ is 17 kcal/mol (calculated from data in Ref. 33.

36. H. A. Weakliem, J. Chem. Phys., 36, 2117 (1962).

37. R. Klucker, H. Nelkowski, Y. S. Park, M. Skibowski, and T. S. Wagner, Phys. Stat. Sol. (b), 45, 265 (1971).

38. V. Rössler, Phys. Rev., 184, 733 (1969).

39. S. Bloom and I. Ortenburger, Phys. Stat. Sol (b), 58, 561 (1973).

40. The theoretical band structures of ZnO calculated by the KKR method (Ref. 38) and pseudopotential method (Ref. 39) are in good agreement except for the position of the Zn 3d band which was taken from Ref. 39 for representation in Figure 21. The Zn 3d band may be lower than indicated [39].

41. This argument is based on the model of G. Leman and J. Friedel, J. Appl. Phys., Supplement to Vol. 33, 281 (1962) for diamond structure semiconductors in the "strong bond" region in which the valence bandwidth is equal to the s-p promotion energy and the bandgap is proportional to nearest neighbor resonance integrals. The model is easily extended to wurtzite structures with the same resulting properties of energy bands, and is fully consistent with valence bandwidths of ZnO, 4-5 eV, obtained from more elaborate theoretical treatments [39,40], being close to the Zn 4s-O 2p atomic level difference, 4.2 eV.

42. G. Heiland, E. Mollwo, and F. Stöckmann, Solid State Phys., 8, 191 (1959).

43. K. Klier, Coll. Czech. Chem. Commun., 27, 920 (1962).

44. R. P. Eischens, W. A. Pliskin, and M. J. D. Low, J. Catal., 1, 180 (1962).

45. R. J. Kokes and A. L. Dent, Adv. Catal., 22, 1 (1972).

46. A. Cimono, E. Molinari, and E. Cipollini, Proc. 2nd Internat. Congr. Catalysis, 1960, p. 263; P. M. G. Hart and F. Sebba, Trans. Faraday Soc., 56, 551 (1960).

47. F. A. Cotton and G. Wilkinson, "Advanced Inorganic Chemistry," 2nd Ed., Interscience Publ., London, 1966, p. 898.

48. Y. Y. Huang, J. Catal., 30, 187 (1973).

49. J. Texter, D. H. Strome, R. G. Herman, and K. Klier, J. Phys. Chem., 81, 333 (1977).

50. The energy of the 3σ orbital of CO is given by its ionization potential, -14.0 eV (cf. H. D. Hagstrum and J. T. Tate, Phys. Rev., 59, 354 (1941)), and that of the π^* orbital is -5.94 eV, as determined from the $A^1\Pi$ state excitation energy (cf. G. Harzberg, "Molecular Spectra and Molecular Structure," Vol. I, 2nd ed., Van Nostrand 1950, p. 452). Thus the direct donation from CO (3σ) orbitals into the Cu^I/ZnO lowest lying empty band with band edge lying above the Fermi level of ZnO, -4.4 eV, has a low probability and hence a small contribution to bonding. On the other hand, the full Cu^+(3d) levels located in the ZnO bandgap between -6 eV and -3 eV have energies equal to or greater than that of the empty CO(π^*) orbital and are thus very well suited for backdonation.

51. S. Tsuchiya and T. Shiba, Bull. Chem. Soc. Jap., 38, 1726 (1965); and references quoted therein.

52. G. Natta in "Catalysis," Vol. III, P. H. Emmett, Ed., Reinhold Publ. Corp., New York, 1955, p. 399.

53. Ref. 52, p. 380; also see P. Davies and F. F. Snowdon, U.S. Patent 3,326,957 (June 20, 1967) and D. Cornthwaite, British Patent 1,296,212 (Nov. 15, 1972) -- both assigned to Imperial Chemical Industries, Ltd.

54. J. Dewing and D. S. Davis, Adv. Catal., 24, 221 (1975).

55. F. J. Bröcker, German Patent 2,116,949 (Oct. 19, 1972); assigned to Badische Anilin- & Soda-Fabrik AG.

56. K. Klier, "Advanced Methanol Synthesis Catalysts," Second Semi-annual Technical Progress Report to ERDA and NSF (RANN), Grant No. AER-75-03776, December 10, 1976.

57. Virtual oxygen pressures at 550°K for CO_2/CO = 6/24 and H_2O/H_2 = 1/100 are 9 x 10^{-46} and 2.5 x 10^{-46} atm, respectively. The oxygen pressure for oxidation of Cu metal to Cu_2O is 4.4 x 10^{-25} atm and for oxidation of atomic dispersion of copper to Cu_2O is less than 10^{-99} atm.